ACTA GEOLOGICA HISPANICA, v. 27 (1992), nº 3-4, pàgs. 13-32

Recent advances in the understanding of mid-ocean ridge tectonics and volcanism using swath-mapping tools

K.C. MACDONALD[1], D.S. SCHEIRER[1], S. CARBOTTE[1] and P.J. FOX[2]

(1) Department of Geological Sciences and Marine Sciences Institute.University of California. Santa Barbara, CA 03106, USA.

(2) Graduate School of Oceanography. University of Rhode Island. Narragansett, RI 02882, USA.

ABSTRACT

New swath mapping sonar systems have revealed the structure of the mid-ocean ridge (MOR) and surrounding deep ocean floor with unprecedent clarity. These images show that the MOR is partitioned into segments by a variety of offsets such as transform faults, overlapping spreading centers and very fine scale discontinuities which are barely detectable. The smallest scale segments are the fundamental building blocks for creation of new oceanic crust. They are only 2-20 km long and are active, distinct units for only ≈100-10,000 years. At fast spreading centers, the axial neovolcanic zone is a persistent 300-400 m high elevation produced by the bouyancy of hot rock and magma; it is not a volcanic construction (most of the time and in most places) so there is almost no vestige of it off-axis. Along ≈60% of its length, the spreading center is characterized by an axial summit caldera produced by volcanic inflation and collapse. The size and shape of the axial high are very sensitive indicators of a relatively steady and robust magma supply at fast-spreading ridges, and have been used successfully to predict the location of magma chambers and to forecast recent volcanic eruptions including one witnessed from ALVIN in March-April 1991. At intermediate spreading rates, the axial region cools sufficiently for a volcanic constructional edifice to develop episodically and for normal faulting to occur along an axial graben. Under these conditions axial volcanoes are split in two by the axial graben and remnants can be found on the flanks of spreading centers. At slow-spreading ridges, the magma budget is relatively starved as indicated by a persistent axial rift valley and a highly discontinuous neovolcanic zone, and strong asymmetry in profiles along and across the strike of the ridge.

Key words: Swath mapping. Mid-ocean ridge. Spreading rate. Segment. Volcanism. Discontinuity. Axial high. Neovolcanic zone.

RESUMEN

En la década de los 60 se produjeron tres avances significativos en el estudio morfológico de los fondos oceánicos: ecosondas de haz estrecho inmergidas cerca del fondo, sonar de barrido lateral y batimetría de barrido de multihaz. Los sistemas de multihaz han sido los últimos puestos a disposición de la comunidad oceanográfica civil, ya avanzada la década de los 70. No obstante, aún hoy la mayoría de datos de multihaz de la U.S. Navy están clasificados, y sólo media docena de buques oceanográficos en el mundo proporcionan libremente datos de multihaz. La importancia de los sistemas de multihaz radica en que permiten medir y cartografiar la morfología del lecho marino con una cobertura espacial completa y una resolución relativamente alta. Las particulares condiciones ambientales en los grandes fondos y, especialmente, en las dorsales medio-oceánicas hacen que los mapas resultantes devengan directamente mapas estructurales, tectónicos y volcánicos, conviertiéndose en elementos imprescindibles para geólogos y geofísicos.

Los mapas batimétricos de multihaz muestran que la dorsal medio-oceánica (DOMO) está desplazada y dividida en segmentos por diversas discontinuidades, como las fallas transformantes, los centros de expansión solapantes y otras discontinuidades de escala mucho menor y más difíciles de detectar. Los distintos tipos de discontinuidades y los segmentos de dorsal que delimitan han sido clasificados jerárquicamente en órdenes de magnitud que van del 1 al 4. Los segmentos de primer orden están limitados por fallas transformantes que permanecen durante millones de años, determinando desplazamientos laterales de decenas a centenares de kilómetros que oponen tramos de dorsal cuya diferencia de edad oscila entre uno y varias decenas de millones de años.

Las discontinuidades de segundo y tercer orden no son estables durante períodos de tiempo largos, y oponen tramos de dorsal separados por menos de un millón de años de edad, y desplazados a lo sumo unas pocas decenas de kilómetros. Existe aún un cuarto orden de seg-

mentación superpuesto a los anteriores, que determina la aparición de formas arcuadas de longitud de onda quilométrica a lo largo del eje de la dorsal.

La integración de datos morfológicos, estructurales, sísmicos y geoquímicos ha llevado a la confección de un modelo de aporte de magma en el que la génesis, el transporte y la distribución de la mezcla fundida procedente del manto superior están reforzadas debajo de la región central, somera e hinchada, de cada segmento y debilitadas en los extremos, cerca de las discontinuidades axiales.

Los segmentos de menor orden constituyen las unidades elementales en la formación de nueva corteza oceánica. Sólo miden entre 2 y 20 km de longitud y sólo persisten, como elementos activos, entre 100 y 10.000 años.

La naturaleza, las características y la evolución de los segmentos varía, no obstante, según la tasa de expansión, desde las dorsales rápidas, como la Dorsal del Pacífico Este, hasta las dorsales lentas, como la Dorsal Atlántica, pasando por las intermedias. En los centros de expansión rápidos, la zona neovolcánica axial está constituida por una elevación persistente, de 300 a 400 m de altura, debida a la flotabilidad de la roca sobrecalentada y del magma. Dicha elevación, cuyas dimensiones y forma indican un aporte sostenido de magma, no es en la mayoría de los casos una auténtica construcción volcánica sino una tumefacción que desaparece cuando, como consecuencia de la separación entre placas, aumenta la distancia al eje de la dorsal. Aproximadamente a lo largo del 60% de su longitud, el eje de expansión está caracterizado por una caldera somital axial, de no más de 500 m de anchura, producida por la propia intumescencia volcánica y el subsiguiente colapso. Las características morfométricas de la elevación axial han sido empleadas con éxito en la localización de cámaras magmáticas, y en la predicción y comprobación de erupciones volcánicas, como las verificadas en varias inmersiones de los sumergibles ALVIN y CYANA en la Dorsal del Pacífico Este desde 1984 hasta la actualidad. Las predicciones basadas en criterios morfométricos han sido, por otra parte, corroboradas por criterios sísmicos obtenidos a partir de la detección del reflector correspondiente al techo de la cámara magmática.

En las dorsales con una tasa de expansión intermedia, el apreciable enfriamiento de la región axial y el mayor grosor de la litosfera de edad cero, permiten el desarrollo episódico y el mantenimiento de auténticos edificios volcánicos constructivos, y la ocurrencia de fallas normales a lo largo de un graben axial. La continuación de la expansión conlleva la partición de los volcanes y el alejamiento progresivo de las mitades resultantes preservadas en los flancos de la dorsal.

En contraste con las dorsales rápidas e intermedias, las dorsales intermedias subalimentadas y las dorsales lentas están caracterizadas por un valle de rift y una zona axial neovolcánica marcadamente discontínua, que son consecuencia de un aporte muy escaso de magma. Los volcanes, formados enteramente por coladas de lava, tienen formas cónicas y son de pequeño tamaño, levantándose en promedio 60 m sobre los fondos adyacentes.

De lo antepuesto se desprende que las diferencias morfológicas en los ejes de las dorsales están directamente relacionadas con los aportes locales de magma y que, en las dorsales rápidas, la estructura detallada de la caldera somital axial está relacionada directamente con la historia eruptiva reciente.

Palabras clave: Cartografía de barrido. Dorsal medio-oceánica. Tasa de expansión. Segmento. Volcanismo. Discontinuidad. Elevación axial. Zona neovolcánica.

SOUNDING THE DEEP OCEAN FLOOR

Great strides have been made in revealing the shape and structure of the ocean floor (Fig. 1). The original soundings of the deep ocean floor were made with hemp ropes in the 1800's and later with wire ropes. With teams of men grunting away at windlasses, a single sounding could take a full day. A major advance was made in the late 1920's with the development of the echo-sounder, a device which emits a burst of sound and measures how long it takes the ping to echo off the seafloor. With this new instrument and a graphic recorder, continuous profiles with a sounding every 10-30 seconds were produced. This system has been used routinely on oceanographic vessels for the last forty-five years. One drawback is that the 60° wide acoustic pulses spread as they travel downward through the ocean, much like the beam of a flashlight, so that the returned sound energy echoes off a very broad region of the seafloor, as large as 3-5 km^2. The resulting depth profile is a very noisy and smoothed representation of the seafloor shape.

Three major advances were made in the 1960's. To achieve better accuracy, echo sounders were developed which had narrower beams and were towed close to the seafloor (Spiess and Tyce, 1973). At only 50 m above the seafloor, the "footprint" of the echo sounder was reduced to 10 m2, so that a very precise profile of the seafloor could be produced. A limitation was the ship speed, which was reduced to only 3 km/hr. Only small areas (< several hundred square kilometers) thought to be diagnostic of important relationships in processes have been mapped in this way. Side scan sonar was developed in which the amplitude of the echoes sound was recorded as a function of time. The strength of the echo is a measure of bottom roughness (backscatter) and slope. The images resemble slightly fuzzy black and white photographs and depending on the depth at which they are towed, create acoustic images with swath widths that range from a few hundred meters to 60 km. In general, there is a trade off between the width of the side scan swath and resolution (Davis *et al.*, 1986). Used in an interferometric mode, side scan sonars such as SeaMARC II can also be used to measure depths in addition to backscatter.

The third advance and the most critical in terms of mapping large areas of the seafloor with high resolution, was the development of the multi-beam echo sounder which produces an array of 16-120 beams which are very narrow (1-3°). The array of beams ensonifies a wide "swath" beneath the ship, 60-300% of the water depth or 1.5-15 km wide for deep water work. Resolution varies from approximately 5 m for near-vertical beams to ≈50 m for echoes 60° from vertical for water depths of 2-6 km (Renard *et al.*, 1991).

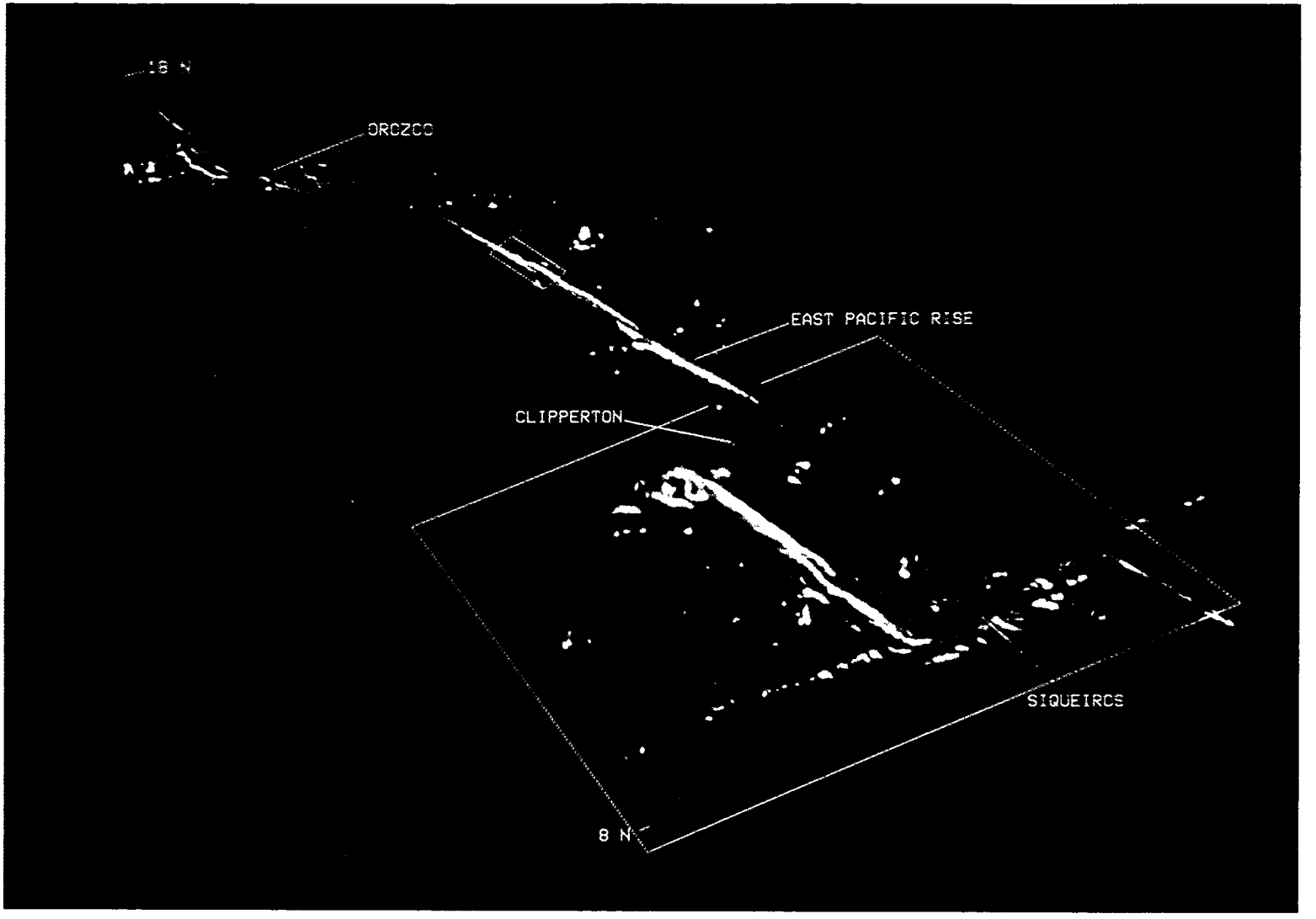

Figure 1.- The fast-spreading East Pacific Rise 8°N-18°N. Shaded relief image view toward NE. White boxes show locations of images in Fig. 4 (foreground) and Fig. 7 (see Fig. 4 for color depth scale). The image is 1100 km long by about 350 km wide. The EPR is the elevated N-S trending region in the red-yellow depth range. The Siqueiros transform is in the foreground followed by the 9°N overlapping spreading centers, the Clipperton transform, the 11°54N OSC and the Orozco transform in the background (image produced at UCSB by S.P. Miller based on data from Macdonald *et al.*, 1992).

Figura 1.- Dorsal rápida del Pacífico Este entre 8°N y 18°N, en una imagen en relieve vista hacia el NE. Los recuadros blancos muestran la posición de las imágenes de la Fig. 4 (en primer término, recuadro grande) y de la Fig. 7 (en segundo término, recuadro pequeño). Véase la escala de profundidades en color en la Fig. 4. La imagen cubre 1.100 km de largo por unos 350 km de ancho. La DOPE es la región elevada de dirección N-S en el rango de colores rojo y amarillo. A la falla transformante de Siqueiros, en primer término, le siguen los centros de expansión solapantes de 9°N, la falla transformante de Clipperton, el CES de 11°45N y la falla transformante de Orozco, en último término (imagen obtenida en la Universidad de California-Santa Bárbara por S.P. Miller a partir de datos de Macdonald *et al.*, 1992).

The importance of multibeam systems is that seafloor shape can be measured with complete spatial coverage while retaining relatively high resolution. No longer must we engage in the artful guesswork of drawing contours connecting points of equal depth, interpolating over tens of kilometers (see Davis *et al.*, 1986; Tyce, 1987, for more complete and detailed reviews and references on seafloor mapping systems). Unfortunately, multibeam systems did not benefit the oceanographic community until the late 1970's, nearly 15 years after their inception, because multibeam maps were cloaked in the secrecy of the U.S. Navy. Even with the demise of the Soviet Union, most of the U.S. Navy multibeam data is still classified; only data from half a dozen civilian and academic ships is generally available to scientists and the public.

High quality topographic maps of many continental regions have been available for some time, so why are we so excited about high resolution continuous coverage charts of the ocean floor? In continental regions, erosion caused by flowing water and ice, as well as wind, scours and shapes the landscape, masking and muting the long and complex influence of tectonics and volcanism on topography. As with the surface of Venus (Head and Saunders, 1991), the relative lack of erosion on the deep ocean floor, and its relative simple history, means that a high resolution bathymetric chart can be translated directly into a map of structure, tectonics, and volcanism. This tool is particularly powerful in mid-ocean ridge regions which are relatively free of sediment burial, and are the birthplace of ≈60% of the earth's crust and lithosphere.

There are many examples of the powers of bathymetric interpretation in understanding fundamental geologic processes. On a global scale, for example, Sclater *et al.* (1971) showed that the depth of the seafloor increases as the square root of its age. This observation showed that the oceanic lithosphere is reasonably approximated by a conductively cooling plate approximately 75 km thick. This observation was also used to predict seafloor age where magnetic anomalies were not interpretable and to locate fossil and jumped spreading centers. We will focus on three examples in which high resolution swath bathymetric maps have helped marine geologists and geophysicists to study the processes operating at mid-ocean ridges.

SEGMENTATION OF THE MID-OCEAN RIDGE

When viewed in an along-axis perspective, the axial depth and continuity of the world-encircling Mid-Oceanic Ridge (MOR) is segmented at various scales and in various ways (Table 1). At the longest wavelengths, the along-strike axial profile of the ridge is characterized by a broad swell with dimensions in excess of 1000 km. The crests of these swells are defined by hot spots, reach anomalously shallow levels, and are associated with excessive and long-lived magmatic budgets. At shorter wavelengths (a few tens to hundreds of kilometers), the global ridge system, independent of spreading rate or proximity to hot spots, is partitioned into discrete segments by a family of ridge-axis discontinuities which have distinctive structural signatures. Because these offsets exhibit dis-

TABLE 1. CHARACTERISTIC OF RIDGE SEGMENTATION

	Order 1	Order 2	Order 3	Order 4
Segments				
Length (km)*	600 ± 300 (400 ± 200)	140 ±90 (50 ± 30)	50 ± 30 (15 ± 10?)	14 ± 18 (7 ± 5?)
Longevity (yr)	>5 x 10^6	0.5 – 5 x 10^6 (0.5 – 10 x 10^6)	~10^4 – 10^4 (?)	~10^2 – 10 (?)
Discontinuities				
Offset (km)	>30	2 – 30	0.5 – 2.0	<1
Age (yr)†	>0.5 x 10^6	<0.5 x 10^6	~0	~0
Off-axis trace	Fracture zone	V-shaped discordant zone	None	None

Table 1.- Characteristics of ridge segmentation (after Macdonald *et al.*, 1991). Information is for fast-spreading (> 60 mm/yr) ridges. If it differs from that for slow-spreading ridges, is in parenthesis.
* Errors are ±1σ.
† The age of seafloor that is juxtaposed to the spreading axis at a discontinuity.

Tabla 1.- Características de los distintos órdenes de segmentación en las dorsales oceánicas (de Macdonald *et al.*, 1991). La información es para dorsales rápidas (> 60 mm/yr). En paréntesis se dan los datos correspondientes a dorsales lentas, si son distintos.
* Los errores son ± 1σ.
† La edad del fondo oceánico que está yuxtapuesto al eje de expansión en una discontinuidad.

tinctive morphologic and geochemical characteristics, both in space and time, they, and the ridge segments that they partition, have been arranged in a hierarchycal classification scheme of orders 1-4 (Figs. 2 and 3) (Schouten *et al.*, 1985; Langmuir *et al.*, 1986; Macdonald *et al.*, 1988; Macdonald and Fox, 1990).

Transform faults define first-order segments, and are large offsets of opposing ridge segments in terms of both distance (tens to hundreds of kilometers) and age (approximately one to tens of millions of years). They link ridge segments along a narrow strike-slip fault zone against which ridge axis parallel terrain truncates (Figs. 1, 4, 5 and 6c). These boundaries are stable for long periods of time (millions of years). Their aseismic extensions describe portions of small circles, and these extensions can be traced as continuous lineaments for hundreds to thousands of kilometers across the flanks of the ridge. Transform fault boundaries will be conditioned by, and will condition, accretionary processes be-

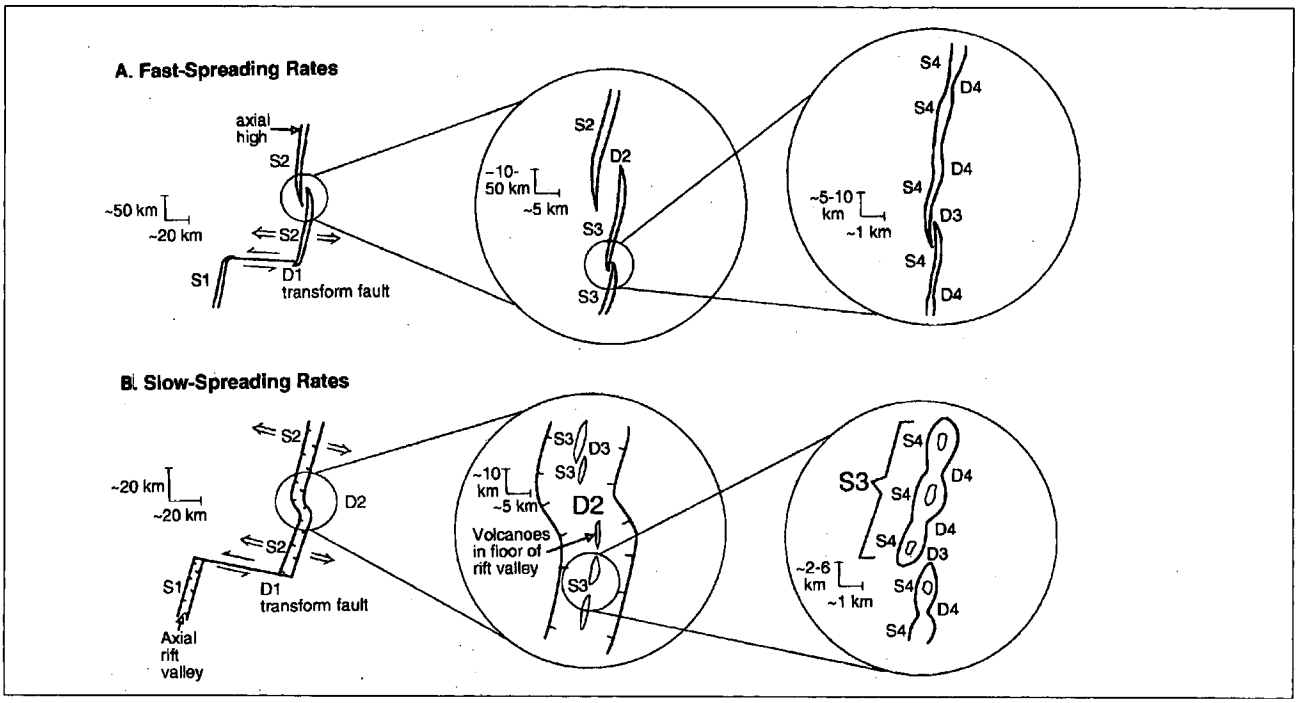

Figure 2.- A proposed hierarchy of ridge axis discontinuities of orders 1 through 4 for slow (bottom) and fast (top) spreading centers (after Macdonald *et al.*, 1991). S1, 2, 3, 4 are ridge segments of order 1, 2, 3, 4 and D1, 2, 3, 4 are ridge axis discontinuities of order 1, 2, 3, 4. Thus a segment is first-order if it is bounded at both ends by first-order discontinuities and second-, third-, or fourth-order if it is bounded at one (or both) end(s) by second-, third-, or fourth-order discontinuities. At both fast- and slow- spresding centers, first-order discontinuities are transform faults. Examples of second-order discontinuities are overlapping spreading centers (OSCs) on fast-spreading ridges and oblique shear zones and intervolcano gaps on slow-spreading ridges. Third order discontinuities are small OSCs on fast-spreading ridges and inter-volcano gaps on slow-spreading ridges. Fourth order discontinuities are deviations from axial linearity (Devals) resulting in slight bends or lateral offsets of the axis of less than 1 km on fast-spreading ridges and are intra-volcano gaps on slow-spreading ridges. The four-tiered hierarchy of segmentation may really be a continuum. It has been established, for example, that fourth order segments and discontinuities can grow to become third-, second-, and even first-order discontinuities and vice-versa at both slow-and fast-spreading centers. Intermediate-rate spreading centers (40-90 mm/yr) tend to have the characteristics of slow-spreading segments and discontinuities when they are magmatically starved, and those of fast-spreading centers when magmatically robust. Even a fast-spreding center can have slow-spreading characteristics temporarily during periods of magma drought.

Figura 2.- Propuesta de jerarquización de las discontinuidades de los ejes de dorsal en cuatro órdenes para centros de expansión lentos (abajo) y rápidos (arriba) (de Macdonald *et al.*, 1991). S1, 2, 3 y 4 designan segmentos de dorsal de orden 1, 2, 3 y 4. D1, 2, 3 y 4 designan discontinuidades axiales de orden 1, 2, 3 y 4. Un segmento es de primer orden si está limitado en ambos extremos por discontinuidades de primer orden, y de segundo, tercer o cuarto orden si está limitado en un (o en ambos) extremo(s) por discontinuidades de segundo, tercer o cuarto orden. Como ejemplos de discontinuidades de segundo orden están los centros de expansión solapantes (CES) en las dorsales rápidas, y las zonas de cizalla oblicua en las dorsales lentas. Como discontinuidades de tercer orden se pueden citar los pequeños CES de las dorsales rápidas y los boquetes intervolcánicos de las dorsales lentas. En las dorsales rápidas, las discontinuidades de cuarto orden consisten en desviaciones de la linearidad axial (Devals) que dan lugar a pequeñas arcuaciones o desplazamientos laterales del eje de menos de 1 km, mientras que en las dorsales lentas consisten en boquetes intravolcánicos. Esta segmentación en cuatro órdenes puede, no obstante, formar un contínuo. Es conocido, por ejemplo, que los segmentos y discontinuidades de cuarto orden pueden crecer y convertirse en discontinuidades de tercer, segundo e, incluso, primer orden, y viceversa, tanto en centros de expansión lentos como rápidos. Los centros de expansión intermedios (40-90 mm/año) tienden a presentar las características de las discontinuidades y segmentos con expansión lenta cuando están magmáticamente subalimentados, y las de los centros con expansión rápida cuando el aporte de magma es vigoroso. Incluso un centro con expansión rápida puede presentar, temporalmente, características propias de la expansión lenta durante fases de escasez de magma.

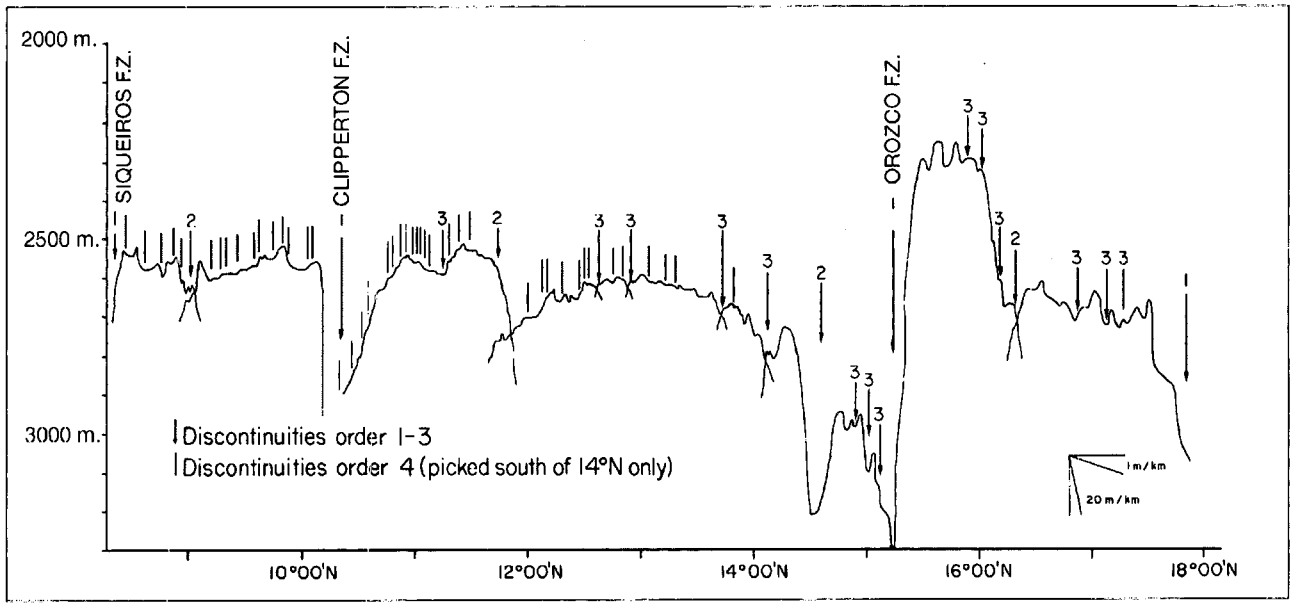

Figure 3.- Axial depth profile of the EPR 8°N-18°N taken from Macdonald *et al.*, (1992). Numbers correspond to ridge axis discontinuities of orders 1 through 3. Fouth-order discontinuities (unlabelled vertical lines) are only identified south of 14°N so the lack of fourth-order discontinuities north of 14°N indicates only that they have not been identified yet. In contrast to discontinuities of order 1-3, fourth order discontinuities have little or no axial depth anomaly.

Figura 3.- Perfil de profundidades axiales de la DOPE entre 8N° y 18°N (de Macdonald *et al.*, 1992). Los números indican las discontinuidades axiales de orden 1 a 3. Las discontinuidades de cuarto orden (líneas verticales sin números) sólo han sido identificadas al sur de 14°N, por lo que la falta de discontinuidades de este orden al norte de esa posición únicamente indica que las mismas aún no han sido reconocidas. En contraste con las discontinuidades de orden 1 a 3, las de cuarto orden corresponden a anomalías en la profundidad axial pequeñas o inexistentes.

cause the fault juxtaposes a barrier of aged lithosphere against the zero-age axis of the ridge segment (Fox and Gallo, 1984).

In contrast, ridge-axis discontinuities of the second- and third-order include a range of offset geometries (e.g. overlapping spreading centers along the East Pacific Rise (EPR); oblique relay zones along the Mid-Atlantic Ridge (MAR) (Searle and Laughton, 1977)), and are small offsets of the opposing ridge segments in terms of both distance (less than a few tens of kilometers) and age (less than approximately one million years) (Figs. 1, 4, 5a and b). At second and third order discontinuities, structures indicative of a through-going zone of shear and rigid plate boundary behavior are not spatially sustained, suggesting that these offset geometries are not stable for long periods of time. These medium order ridge-axis discontinuities are caused by differential asymmetric spreading, small changes in spreading direction, and variations in the process of melt generation (Lonsdale, 1989; Perram and Macdonald, 1990). The distinction between second- and third-order offsets is that the magnitude of a third-order offset is relatively small (< a few kilometers), and there is little or no trace of third order features off-axis (i.e. third order segmentation is not long-lived, < 10^5 yrs) (Fig. 7a).

The traces of second-order discontinuities are found as swaths of disturbed terrain flanking the ridge axis (called discordant zones), and generally do not trace small circles about the pole of opening (Figs. 4, 5a and b). Second-order segmentation patterns can follow one of at least two evolutionary paths: They migrate along-strike leaving a V-shaped wake of abandoned ridge tips and basins; or they may remain approximately in the same place, but oscillate back and forth along the ridge (Lonsdale, 1985; Macdonald *et al.*, 1987; Wilson, 1990). It has been documented along the fast end of the accretionary spectrum (EPR) that these discontinuities form abruptly, migrate rapidly along strike at variable velocities and directions, and are short-lived (less than a few million years) (Macdonald *et al.*, 1988; Carbotte and Macdonald, 1992). Along-strike propagation speeds of up to 4000 mm/yr have been documented on the EPR near 18°S (Cormier and Macdonald, 1991). Although less well constrained at the slow end of the accretionary spectrum (< 40 mm/yr), second order discontinuities appear to be longer-lived (millions of years), propagate less rapidly, and exhibit a range of behavior in terms of spatial positioning (Sempéré *et al.*, 1990; Fox *et al.*, 1991). They can remain fixed or they can migrate along strike creating V-shaped patterns characterized by obliquely oriented ridges and basins. At all spreading rates, it is possible for one type of ridge-

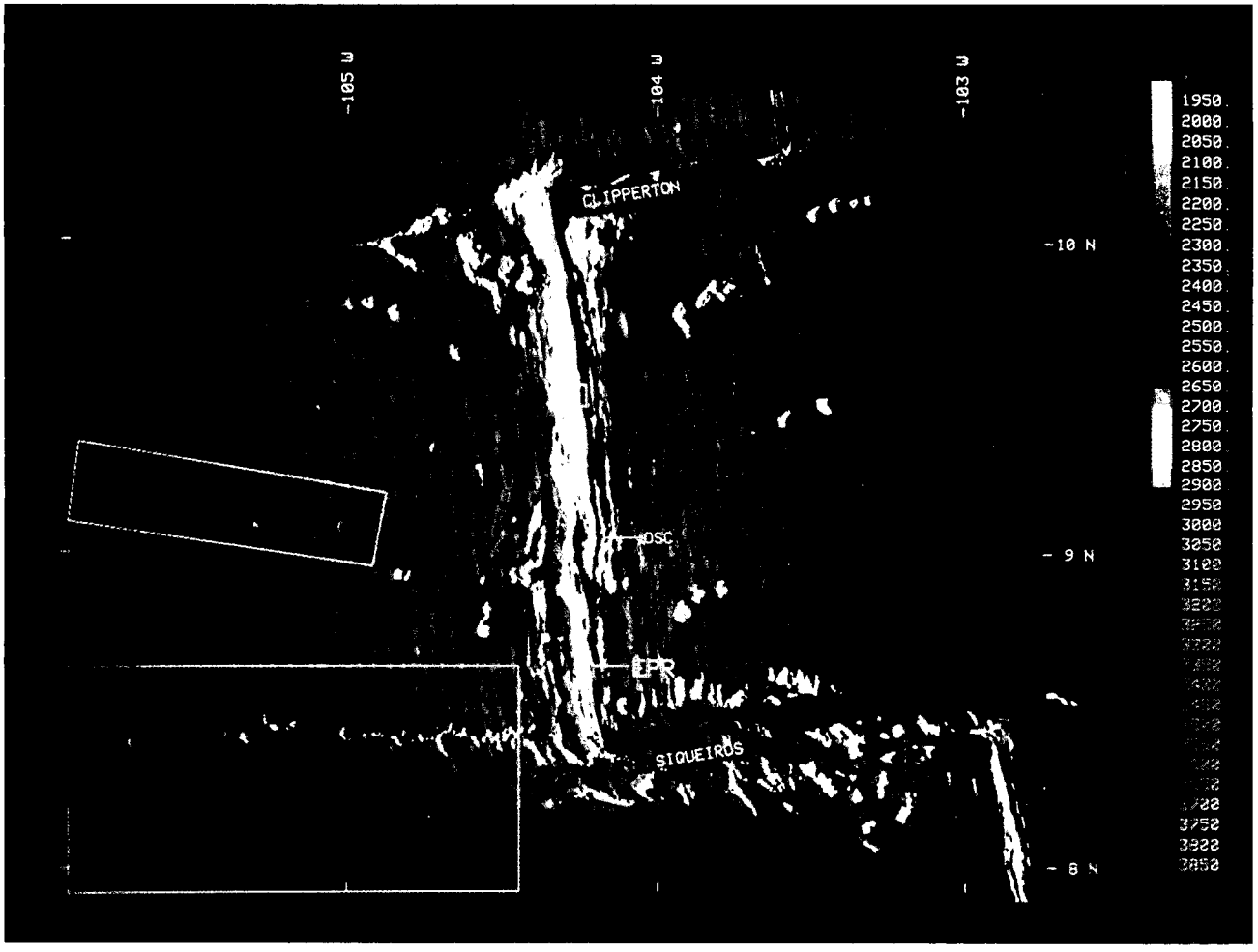

Figure 4.- Merged SeaBeam and SeaMARCII bathymetry in the Office of Naval Research East Pacific Rise Natural Laboratory (image produced at UCSB by S.P. Miller based on data from Macdonald *et al.,* (1992). Subtle NE-SW grain is an artifact of SeaMARCII bathymetry parallel to the ship track. East Pacific Rise (EPR), 9°N overlapping spreading centers (OSC), Clipperton and Siqueiros transform faults are labelled. Boxes show locations of side scan sonar images of Figs. 6a, b and c. There are no clear vestiges of the 300-400 m high axial region of the EPR on the rise flanks; as it cools the shallow elevation disappears. Lineated N-S relief on the flank is produced by normal faulting (dip toward and away from the axis) and minor volcanism. On the ridge flanks adjacent to the 9°N OSC, a V-shaped discordant zone indicates southward migration of the discontinuity at 52 mm/yr within the past million year. The west flank discordant zone comprises abandoned curvilinear ridge tips that reflect episodic clipping of the western ridge tip at the OSC. The east flank discordant zone consists of greater depths. Southward migration of the discontinuity has not been steady but has involved a series of episodic and dueling propagation events with rates ranging from less than 10 mm/yr to greater than 500 mm/yr.

Figura 4.- Resultado de la integración de batimetrías de SeaBeam y de SeaMARC II efectuado en la "Office of Naval Research East Pacific Rise Natural Laboratory" (imagen obtenida en la Universidad de California-Santa Bárbara por S.P. Miller a partir de datos de Macdonald *et al.,* 1992). El suave grano de dirección NE-SW que se observa en la imagen es un artifacto de la batimetría de SeaMARC II, paralelo a los rumbos del buque. Se han etiquetado la DOPE, los CES de 9° N, y las fallas transformantes de Clipperton y Siqueiros. Los recuadros señalan la localización de las imágenes de sonar de barrido lateral de las Figs. 6a, b y c. En los flancos de la dorsal no hay evidencias claras de la región axial de 300-400 m de altura de la DOPE; a medida que aquélla se enfría, la elevación desaparece. El relieve de orientación N-S que se observa en los flancos es debido a fallas normales (que buzan hacia dentro y hacia afuera del eje) y a volcanismo menor. También en los flancos, cerca del CES de 9° N, una zona discordante en forma de V indica la migración de la discontinuidad hacia el sur, a una velocidad de 52 mm/año durante el último millón de años. La zona discordante del flanco occidental contiene extremos abandonados curvilíneos de dorsal que reflejan cercenamientos episódicos del extremo de la dorsal occidental en el CES. Las profundidades son mayores en la zona discordante del flanco oriental. La migración de la discontinuidad hacia el sur no ha sido regular, sino que ha comportado una serie de eventos de propagación compulsivos a velocidades que han oscilado entre menos de 10 mm/año y más de 500 mm/año.

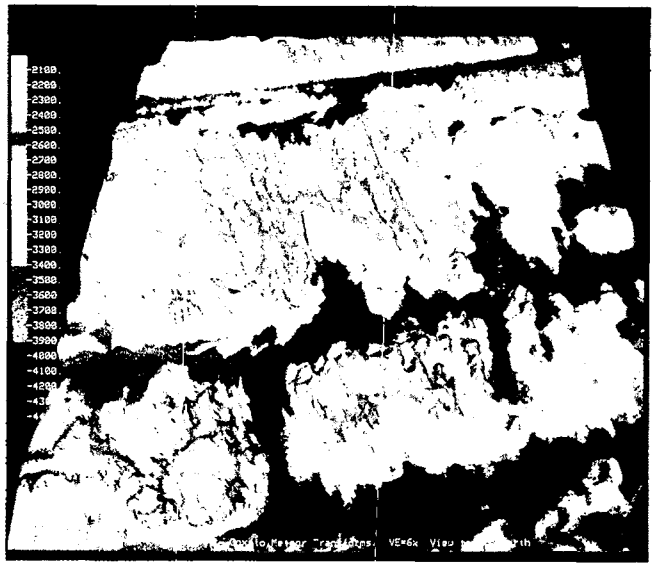

Figure 5.- Images of the slow-spreading Mid-Atlantic Ridge (MAR):

Figura 5.- Imágenes de la Dorsal Medio-Atlántica (DOMA), caracterizada por una expansión lenta:

a) Shaded relief image of slow-spreading southern MAR (31°S-34°S) looking NE. Meteor transform is in the foreground, then the 33°30S second-order discontinuity, Cox transform in background. An axial rift valley marks the spreading axis; it shoals to 200 m deep along 20% of the length of the segment shown but does not disappear (image produced at UCSB by Charles Weiland using data from Fox *et al.*, 1991).

a) Imagen en relieve, vista hacia el NE, de un tramo de la DOMA meridional comprendido entre 31°S y 34° S. La falla transformante de Meteor aparece en primer término, seguida de la discontinuidad de segundo orden de 33°30S, y de la falla transformante de Cox, en último término. Un valle de rift axial señala la posición del eje de expansión; a lo largo de una distancia equivalente al 20% del segmento que se muestra, su profundidad disminuye apreciablemente aunque no llega a desaparecer en ningún momento (imagen obtenida en la Universidad de California-Santa Bárbara por C. Weiland a partir de datos de Fox *et al.*, 1991).

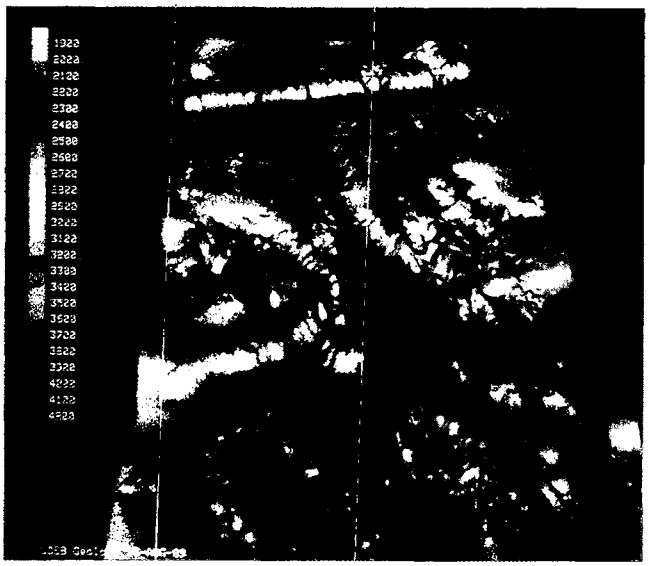

b) Shaded relief image; Cox transform in background; 31°20S second-order discontinuity in foreground (a 12 km right lateral jog of the axial rift valley). View toward S (image produced at UCSB by Suzanne Carbotte using data from Grindlay *et al.*, 1991).

b) Imagen en relieve, vista hacia el S, de un tramo de la DOMA meridional. Se observan la falla transformante de Cox, al fondo, y la discontinuidad de segundo orden de 31°20S, en primer término (con un desplazamiento lateral, de 12 km hacia la derecha, del valle de rift axial) (imagen obtenida en la Universidad de California-Santa Bárbara por S. Carbotte a partir de datos de Grindlay *et al.*, 1991).

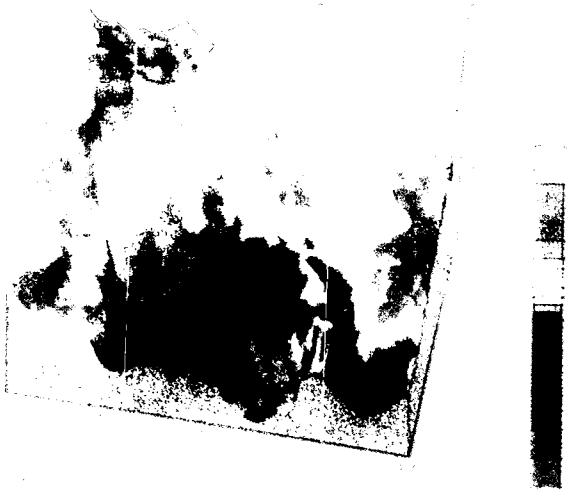

c) Blow-up map of the neovolcanic zone within the axial rift valley from Fig. 5b (10 m contour interval). Note the many small conical volcanoes similar to those observed in N. Atlantic (Smith and Cann, 1990) (image produced at UCSB by Charles Weiland using data from Fox *et al.*, 1991)

c) Mapa ampliado de la zona neovolcánica situada dentro del valle de rift axial de la Fig. 5b (equidistancia, 10 m). Obsérvense los numerosos pequeños volcanes cónicos semejantes a los identificados en el Atlántico Norte (Smith y Cann, 1990) (imagen obtenida en la Universidad de California-Santa Bárbara por C. Weiland a partir de datos de Fox *et al.*, 1991).

axis discontinuity to evolve into another by sustained asymmetric spreading of adjoining ridge segments (Perram and Macdonald, 1990; Grindlay *et al.,* 1991). Characteristically, the terrain in close proximity to the discordant zones is highly magnetized, probably reflecting the eruption of highly fractionated basalts (Carbotte and Macdonald, 1992).

The different types of boundaries outlined above partition the MOR into ridge segments of variable lengths (tens of kilometers to hundreds of kilometers). Independent of length, most ridge segments have arched along-strike topographic profiles, i.e., a depth minimum is located approximately midway along the ridge segment and depths increase towards the ends of the segment (Fig. 3). Each ridge segment is characterized by its own distinctive along-strike profile in terms of relief and gradient from central high to segment ends, and depth of the central high. The extent to which axial depths increase from central high to segment ends ranges from tens to thousands of meters with the largest changes in relief associated with ridge segments along more slowly accreting ridges (e.g. MAR). At fast-spreading ridges, which usually exhibit axial highs, the axial high increases steadily in cross-sectional area with increasing proximity to the elevated mid-sections of individual segments (Macdonald and Fox, 1988; Scheirer and Macdonald, in press).

The scale of ridge segmentations discussed above is relatively easy to recognize because the ridge-axis is clearly offset along strike. Recent high resolution imaging and sampling of the ridge axis in some areas has defined morphologic, bathymetric and geochemical changes along strike that suggest a finer, fourth-order scale of segmentation that is superimposed on the tens to hundreds of kilometer-long segmentation discussed above (Fig. 2) (Langmuir *et al.,* 1986). The along-strike arch-shaped architecture is retained at this small scale but the wavelength is on the order of kilometers and the relief is low. Individual fault traces and volcanic structures along the axis often reflect these deviations in axial linearity by exhibiting right- or left-stepping (<1 km) *en échelon* patterns (Figs. 6a and 7b).

A host of geological observations including the regular undulation of the crest of the ridge, which correlates with its cross-sectional area (Scheirer and Macdonald, in press), seismic evidence for an axial melt reservoir (Detrick *et al.,* 1987; Vera *et al.,* 1990; Harding *et al.,* 1993; Toomey *et al.,* 1990), geochemical anomalies, and the locations of discontinuities has led to the development of a magma supply model for ridge segmentation. In the magma supply model, the generation, transport and distribution of melt from the upper mantle is enhanced beneath the shallow, swollen region of each segment and is depleted at the ends of each segment near overlapping spreading centers (OSCs) and other discontinuities (Macdonald *et al.,* 1991; Langmuir *et al.,* 1986; Sinton and Detrick, 1992; Solomon and Toomey, 1992). As the plates spread apart, partial melting of mantle rocks occurs due to adiabatic decompression at depths of 30 to 60 km. The buoyant melt segregates from residual solid mantle and ascends to fill shallow magma chambers within the crust along the ridge axis. These melts locally swell the crustal magma reservoirs, and buoyant forces associated with the melt and a surrounding halo of hot, melt-impregnated low-density rock create a local shoaling of the ridge crest. Continuous injection of melt leads to local eruptions, migration of magma away from the locus of upwelling, and expansion of the axial magma chamber along strike.The laterally migrating magma loses hydraulic heat with increasing distance from the center of magma replenishment; as a result the depth of the ridge axis steadily increases along strike. As magma migrates at depth along the ridge, continued extension fractures the overlying brittle carapace of frozen lava. Magmas then use these fractures as conduits to the seafloor and volcanic eruptions follow the advancing crack front. The process outlined above occurs repeatedly as plate separation continues. In this magmatic model for a spreading center, ridge-axis discontinuities occur at the distal ends of magmatic pulses and define the ends of ridge segments (Figs. 3a and 5a).

At slow-spreading ridges, seismic studies have not revealed a magma reservoir (Detrick *et al.,* 1990). However, a similar pattern of segmented upwelling may still occur there, and very small pockets of melt or highly episodic magma chambers may be present (Smith and Cann, 1990). Large "bulls-eye"-shaped gravity anomalies occur over ridge segments defined by second-order discontinuities on the MAR (Lin *et al.,* 1990; Kuo and Forsyth, 1988; Blackman and Forsyth, 1991). Corrected to remove the gravitational effects of topography, these anomalies indicate that low-density upper mantle or thickened oceanic crust is present beneath the midsections of segments. Kuo and Forsyth (1988) proposed that these anomalies are best explained by a three-dimensional pattern of upwelling hot mantle material. The pattern of mantle upwelling may become less three dimensional (Lin and Phipps Morgan, 1992), and magma migration within axial magma reservoirs may be more efficient at higher spreading rates (Cochran *et al.,* 1993).

VOLCANISM ON MID-OCEAN RIDGES

The narrow ribbon of active volcanism along spreading axes is called the neovolcanic zone (Macdonald, 1982). The neovolcanic zone is characterized by elongate axial highs tens of kilometers long at fast spreading centers (Searle, 1984); generally shorter (depending on local magmatic budget), discontinuous volcanoes at intermediate rates (Luyendyk and Macdonald, 1985); and a coalesced patchwork of hundreds of small conical to

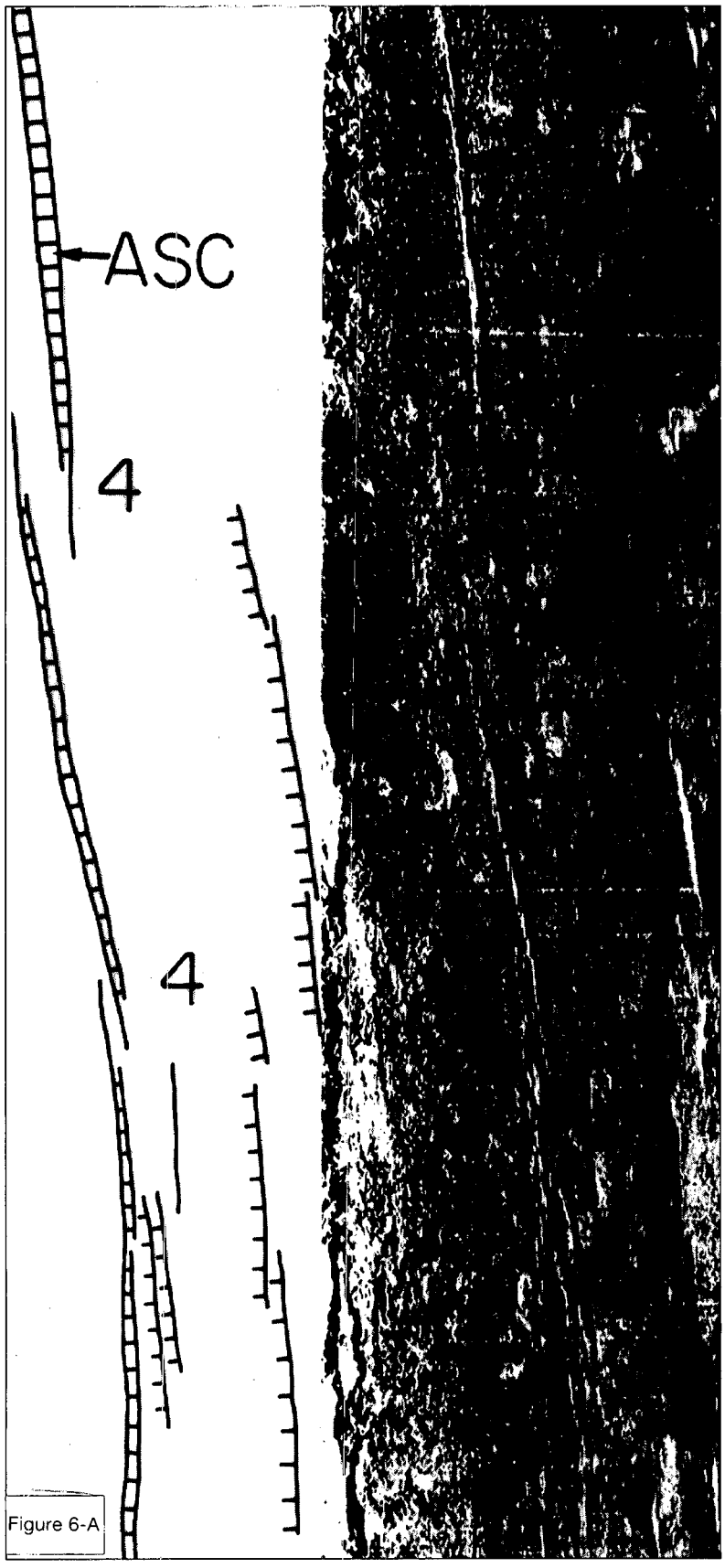

Figure 6-A

Figure 6.- Side scan sonar close-ups and interpretations from Fig. 4; dark areas have a high acoustic reflectivity; white lines show the ship track.

Figura 6.- Ampliaciones en imágenes de sonar de barrido lateral de los sectores recuadrados en la Fig. 4. Las zonas oscuras tienen reflectividades acústicas elevadas; las líneas blancas indican los recorridos del buque.

a) Axial summit caldera (ASC) 9°30N-9°40N; "4's" show the locations of two fourth order discontinuities which offset the ASC less than 1 km; faults are indicated by hachured lines, hachures on the downdropped side.

a) Caldera somital axial (CASA) entre 9°30N y 9°40N, indicada con las siglas ASC (véase texto); los cuatros indican la situación de dos discontinuidades de cuarto orden que desplazan la CASA menos de 1 km; las fallas están indicadas mediante el símbolo habitual, con el labio hundido en la dirección hacia la que apuntan las púas.

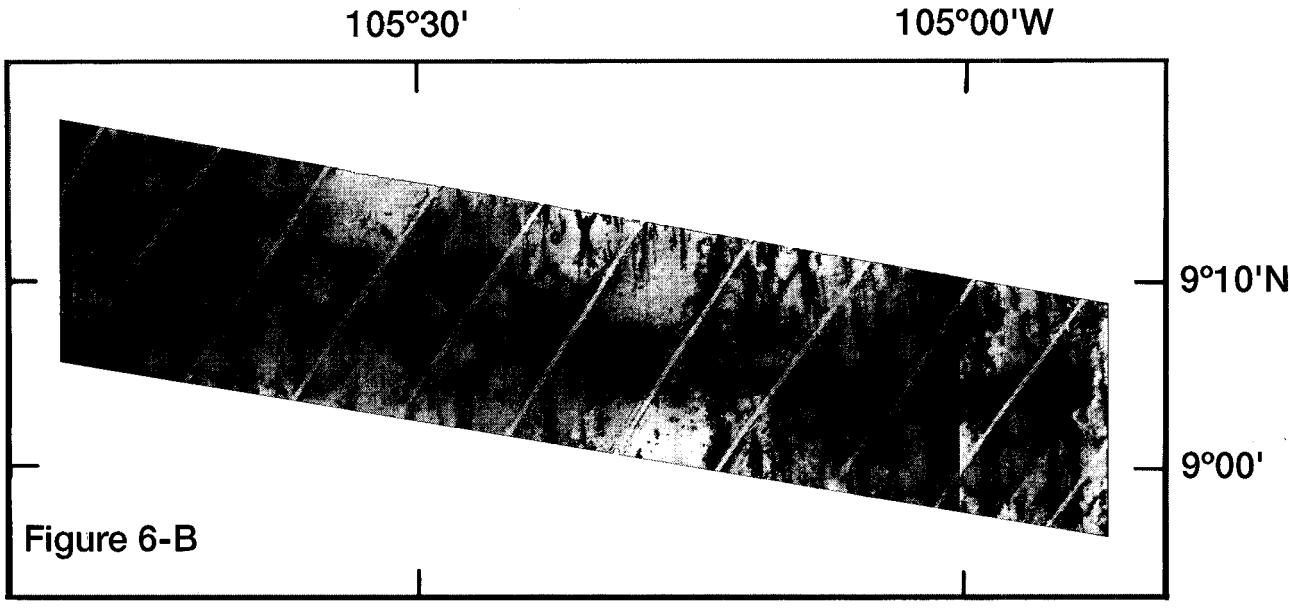

b) Seamount chain; the highly reflective hollows around the seamounts indicate lava flows which are younger than the crust they lie upon.

b) Cadena de montes submarinos cuyos halos altamente reflectivos corresponden a coladas de lava más jóvenes que la corteza sobre la que reposan.

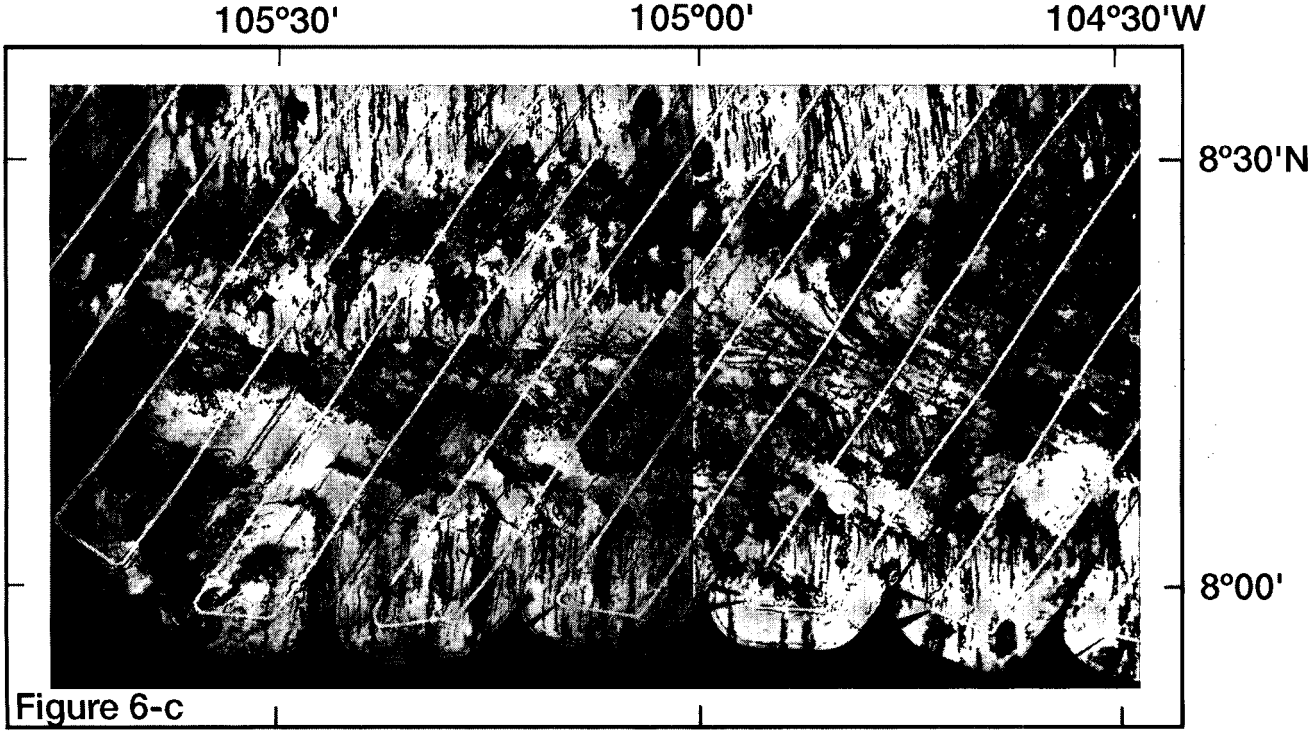

c) West flank of the Siqueiros fracture zone showing history of intra-transform spreading and Southward propagation of EPR cutting across the transform, consuming one of the intra-transform spreading centers (near 8°15N, 104°40W). Also shown is the 8°20N seamount chain.

c) Flanco occidental de la Zona de Fractura de Siqueiros que ilustra una expansión intra-transformante y la propagación hacia el sur de la DOPE cortando a la propia transformante y consumiendo uno de los centros de expansión intra-transformantes (cerca de 8°15N y 104°40W). También se observa la cadena de montes submarinos de 8°20N.

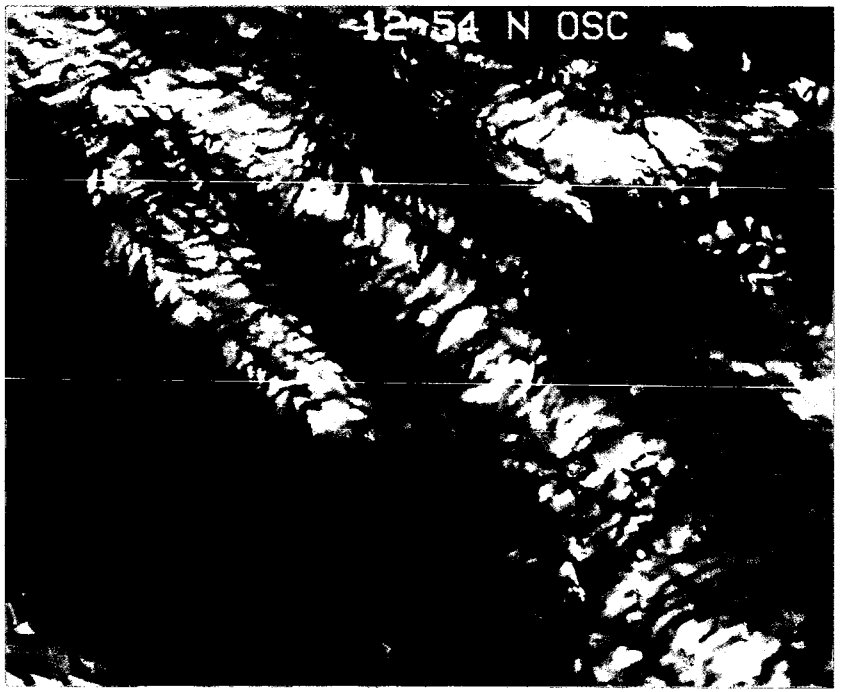

Figure 7.- a) Enlarged shaded image (location in Fig. 1) is the fast spreading EPR 12°35N and 13°N. The 12°37N OSC is in the foreground; 12°54N OSC is in the background. The axial summit caldera is large enough here (≈500 m wide x 50 m deep) to show up as a small axis parallel trough at the crest of the EPR (image produced at UCSB by S.P. Miller based on data from Macdonald *et al.*, 1992).

Figura 7.- a) Imagen en relieve ampliada (véase situación en la Fig. 1) de la dorsal rápida DOPE entre 12°35N y 13°N. El CES de 12°37N aparece en primer término, y el de 12°54N en la parte central de la imagen. La caldera somital axial es aquí bastante grande (≈500 m de ancho x 50 m de profundidad) y se muestra como un pequeño surco axial situado sobre la cresta de la DOPE (imagen obtenida en la Universidad de California-Santa Bárbara por S.P. Miller a partir de datos de Macdonald *et al.*, 1992).

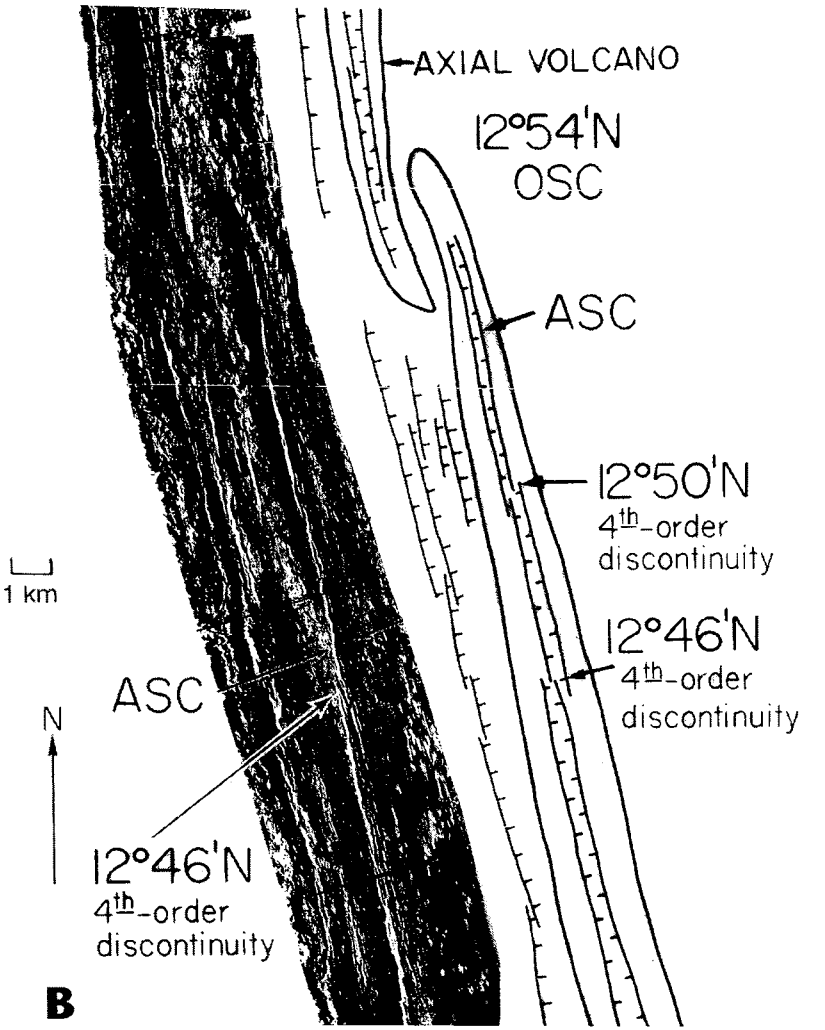

Figure 7.- b) Side scan sonar image and tectonic sketch of EPR 12°40N-13°N showing ASC and examples of third-order (12°54N OSC) and fourth-order (12°50N, 12°46N) discontinuities.

Figura 7.- b) Imagen de sonar de barrido lateral y esquema tectónico de la DOPE entre 12°40N y 13°N mostrando la CASA y discontinuidades de tercer (CES de 12°54N) y cuarto orden (12°50N y 12°46N).

slightly elongate volcanic constructions at slow spreading rates (Smith and Cann, 1992). It is so narrow (≈1-3 km) that axial volcanoes are occasionally split in two and rafted away as the plates separate (Fig. 8) (Macdonald *et al.*, 1980, 1983; Kappel and Ryan, 1986). Yet the most extensive high-resolution study of a fast-spreading ridge to date shows that there are very few structures on the flanks of the EPR which resemble the 300-400 m axial high or split halves of it. The EPR axial elevation seems to disappear completely off-axis (Fig. 4). How can this be? The answer to this question becomes clear when one considers how the neovolcanic zone varies with spreading rate and magma supply.

The axial high on fast spreading centers indicates that the supply of magma is steady and robust, and is able to keep up with the rate of plate separation (Fig. 4). The shape and cross-sectional area of the axial high are sensitive indicators of the local magma supply. The reduction in cross-sectional area and change in shape to a narrow triangular cross-section near many discontinuities indicates a reduction in magma supply near the ends of ridge segments; conversely, magma supply is generally greater along the mid-sections of segments (Macdonald and Fox, 1988; Scheirer and Macdonald, in press). Active volcanism is dominated by linear fissure eruptions along the crest of the rise and extensive outpourings of sheet flows (Choukroune *et al.*, 1984; Macdonald *et al.*, 1989). These lavas erupt from a long, linear trough which occurs along the crest of the axial high (Figs. 5a, 7a and b). This trough is referred to as an axial summit caldera because it is produced by collapse of the frozen volcanic carapace when underlying magma drains away, rather than by block faulting (Haymon *et al.*, 1991a). The caldera is tens of kilometers long and typically ≈50-500 m wide (Macdonald *et al.*, 1984; Searle, 1984). Occurrence of the axial summit caldera (Macdonald and Fox, 1988) coincides almost perfectly with a bright, phased-reversed seismic reflector (Detrick *et al.*, 1987; Harding *et al.*, 1993) which is interpreted to be the roof of a crustal magma chamber beneath the rise. The caldera is also restricted to 60% of the rise where the shape and cross-sectional area indicate a robust magmatic budget, i.e., not near discontinuities of orders 1-3.

The axial high on fast spreading centers has been compared to terrestrial shield volcanoes (Lonsdale, 1977). While this is a very fruitful analogy in understanding the structure and morphology of many submarine volcanic products, this analogy can be misleading because the axial high is not a volcanic construction clear down to the Moho as is Hawaii, for example. Rather, as outlined in the preceeding section, the elevation of the axial high is created primarily by the buoyancy of hot rock and magma which upwell beneath the rise. For example, if the magma supply to Hawaii were cut off, the island would sink beneath the waters of the Pacific due to subsidence of the lithosphere on which it rides, however it would not disappear as it follows the evolutionary path of its predecessors along the Hawaii-Emperor seamount chain. In contrast, the axial high at fast spreading centers will disappear if cut off from its magma supply (Macdonald, 1990). The thickness of the accumulated volcanics is actually thinnest along the axis where the elevation is greatest (Christeson *et al.*, 1992). Thus, while the axial high looks like a shield volcano, it is actually more akin to a long, skinny magma-filled balloon whose diameter is a sensitive measure of magma supply. This is why we see little vestige of the axial "volcano", split or whole, on the flanks of the EPR. As it splits in two, moves off axis and cools, most of it disappears. Only a muted representation of the axial neovolcanic zone survives off-axis (Figs. 1 and 4) (Tighe and Fox, 1991), most commonly within the discordant zones of second order discontinuities where abandoned ridge tips may be supported by thicker lithosphere (Fig. 4).

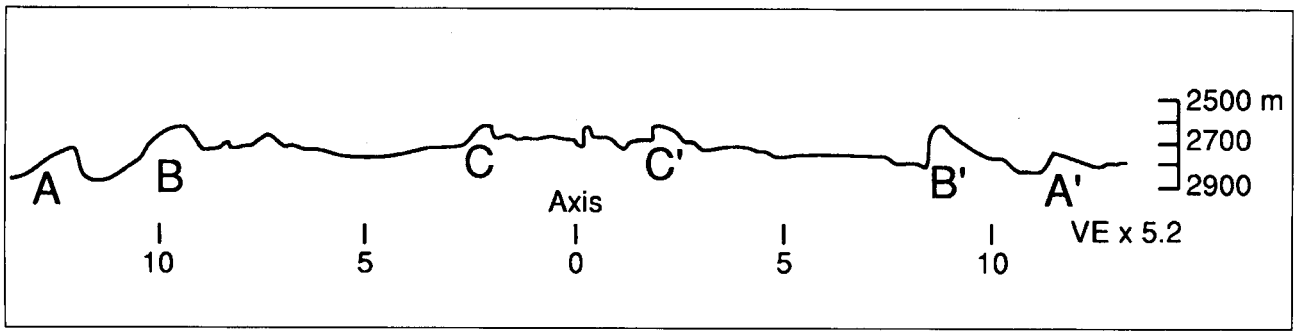

Figure 8.- Deep-tow profile of the intermediate spreading rate EPR near 21°N (Normark, 1976). A-A', B-B' y C-C' represent possible split volcanic edifices, common at intermediate-rate spreading centers but rare at fast-spreading centers (see Fig. 4 and text for discussion).

Figura 8.- Perfil "deep-tow" de un tramo de la DOPE próximo a 21°N, con tasa de expansión intermedia (Normark, 1976). A-A', B-B' y C-C' constituyen posibles edificios volcánicos partidos y separados, frecuentes en los centros con tasa de expansión intermedia y muy raros en los centros con tasa de expansión rápida (véase Fig. 4 y texto).

In contrast, significant volcanic constructional edifices may develop on the ridge axis at intermediate-rate spreading centers (40-90 mm/yr). A more episodic magma supply (Macdonald, 1982) combined with thicker zero-age lithosphere (Purdy *et al.*, 1992) allows axial volcanoes to be constructed and supported along the spreading axis. This thicker zero-age lithosphere also provides sufficient overburden so that normal faulting may occur right along the spreading axis (as opposed to tensional failure and collapse along the axes of most fast-spreading centers where the lithosphere is not sufficiently thick for normal faulting to occur until it has moved 2-5 km offaxis (Carbotte and Macdonald, 1990). Thus, as spreading continues, the episodically forming axial volcano on intermediate-rate spreading centers splits by normal faulting and the two halves of the volcano are rafted away and preserved on the flanks, creating the "bow forms" found by Kappel and Ryan (1986). A direct test of this split volcano hypothesis is that the volcanic section (layer 2A) of the oceanic crust should be thicker beneath abyssal hills than the intervening valleys at intermediate-rate spreading centers, but should have a relatively uniform thickness independent of abyssal hills on fast-spreading centers. Seismic data at fast (Kappus *et al.*, 1992; Harding *et al.*, 1993) and at intermediate-rate spreading centers (Rohr *et al.*, 1992) support this hypothesis. These data also support topographic observations that some of the abyssal hill topography flanking intermediate-rate spreading centers (Fig. 8) may have a volcanic constructional component while the relief associated with lineated hills flanking the fast-spreading EPR is primarily faulted in origin (Lonsdale, 1977; Bicknell *et al.*, 1988; Carbotte and Macdonald, 1990).

In contrast to magmatically robust fast- and intermediate-rate spreading centers, magmatically starved intermediate- and slow-spreading centers are characterized by a rift valley and an axial neovolcanic zone which is discontinuous (Figs. 5a and b) (Macdonald, 1986). Some have argued that the rift valley disappears episodically on slow-spreading ridges, so we have included one of the touted examples of this disappareance in Figure 5a. The rift valley does not disappear along the entire segment; it is over 400 m deep along 80% of its length. Near mid-segment, however, the valley shoals to a 200 m deep half-graben, but even here it does not vanish. At slow-spreading ridges, the axial rift valley disappears along entire segments only near hot spots (e.g. Azores and Iceland) and where rare occurrences of seamount volcanism along the axis overprint the rift valley (e.g. near 26°S, Grindlay *et al.*, 1991).

SeaBeam charts show that the neovolcanic zone within the rift valley inner floor is dotted by numerous small, conical volcanoes averaging 60 m in height (Fig. 5c) (Kong *et al.*, 1988; Smith and Cann, 1992), and less frequently by long, linear volcanic ridges (Pockalny *et al.*, 1988). In contrast to the buouyantly supported axial high at fast-spreading centers, these edifices are true volcanic constructions whose elevations are produced entirely by lava flows, primarily pillow flows (Bryan and Moore, 1977). These discontinuous conical volcanoes suggest point source volcanism from many isolated pockets of magma, in contrast to the remarkably continuous magma reservoir beneath fast spreading centers. Smith and Cann (1992) suggest than hundreds of these volcanoes coalesce to create the volcanic layer on slow-spreading ridges. If so, then the crust created at slow spreading centers is a heterogeneous patchwork of lozenge-shaped volcanic units in contrast to the more continuous "conveyor belt" style of volcanism at fast spreading centers. As at intermediate-rate spreading centers, these volcanoes occasionally split in two (Atwater, 1979), but more often are dismembered with only parts of the volcanoes being preserved as "lips" at the edges of large fault blocks (Macdonald and Luyendyk, 1977; Ballard and van Andel, 1977).

USING TOPOGRAPHY TO FORECAST SEAFLOOR VOLCANIC ERUPTIONS AND AXIAL MAGMA CHAMBERS

Based on SeaBeam maps of the EPR between 9°N-13°N, we suggested that the shape and cross-sectional area of a fast-spreading rise is an indirect measure of its magma supply (Macdonald *et al.*, 1984). A narrow "triangular" cross-section indicates a starved magma supply, while a broad "domed" or "rectangular" cross-section indicates a robust supply of magma. In 1987, Detrick *et al.* published multi-channel seismic results which were consistent with this hypothesis. A bright, phase-reversed reflector, interpreted to be the roof of a narrow crustal magma chamber was observed 1.2-2.0 km beneath the seafloor where the rise axis is domed or rectangular in cross-section, but was absent where the profile is triangular. Furthermore, we found an excellent correlation between the presence of an axial summit caldera (then called an "axial summit graben") and the magma chamber reflector (Macdonald and Fox, 1988). In only two locations between 9°N and 13°N (9°42N-9°55N and near 10°N) did we observe a magmatically robust, dome ridge cross-section, underlain by a bright magma chamber reflector, that was lacking a summit caldera (Fig. 9). We reasoned that these two anomalous locations were in a magmatically robust phase, swollen with underlying magma and smoothed by fresh lavas that had not yet collapsed to form a caldera. Such a location seemed to be a good candidate for a ridge which is in active eruptive phase of its evolution (Macdonald and Fox, 1988).

In 1989, Haymon *et al.* (1991a) conducted a detailed ARGO visual survey of the EPR 9°09N-9°54N for an Ocean Drilling Program site survey. Where we had noted the absence of an axial summit caldera in 1987, the-

re existed in 1989 a narrow caldera (40-70 m wide). Our SeaMARC II survey in 1987 did not detect the feature, indicating that it was either too small to detect with SeaMARC II (unlikely) or that caldera collapse had occurred between 1987-89. During a return submersible program to the same area in April 1991, divers in ALVIN witnessed many indications that an eruption was occurring beneath and around them (Haymon *et al.*, 1991b and submitted). Thriving colonies of tube worms documented to exist during the 1989 ARGO survey were largely buried in fresh glassy lava, but there were scattered about a few scorched corpses. Crabs and other mobil predators were absent in April 1991, but were voraciously feasting on broiled tube worms in May (Haymon *et al.*, 1991c). Large (≈100 m^2) white bacterial mats grew around new hydrothermal vents. High temperature fluids issued forth directly from cracks in the fresh lava flows; there had been no time for fast-growing sulfate/sulfide edifices to form. Based on $^{210}Po/^{210}Pb$ dating, the basalt samples collected at 9°50.6N from ALVIN during April 1-14, 1991 must have erupted during March 26-April 6, 1991 (Rubin and Macdougall, 1991). Evidence of eruption was found at several sites extending throughout the 9°45N-9°52N interval forecasted in 1988 (Haymon *et al.*, 1991c), and appeared to have propagated along an eruptive fissure north to at least 9°54N.

Bouyed by this one apparent forecast success, we inspected our southern EPR SeaMARC II data and found two more sites where we believe eruptions are occurring or will occur very soon; near 14°30S and between 17°20S-17°30S (Macdonald, 1991). The significant maximum in cross-sectional area (Fig. 10) and a ≈20 km stretch where the axial summit caldera is filled and not yet collapsed convinced us that the case for 17°20S-17°30S was particularly compelling, so that area was presented as our next forecast at the 1991 Fall AGU meeting. In the same AGU session, Detrick and Harding presented the first multi-channel results for the very fast-

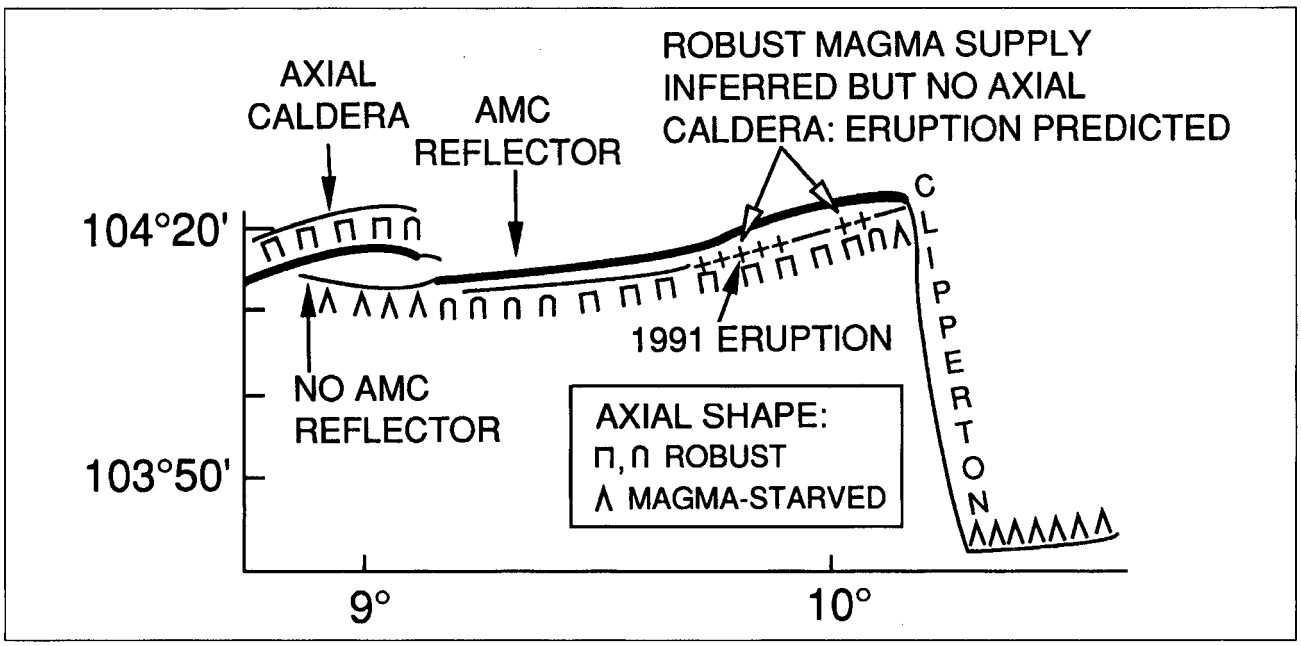

Figure 9.- Enlargement of Macdonald and Fox (1988) Fig. 2 showing basis for forecast of 1991 eruption. Thick line shows location of axial magma chamber seismic reflector (from Detrick *et al.*, 1987), axial shape indicative of robust or starved magma supply as shown, thin line parallel to axis shows where an axial caldera is present, "+" shows the regions where a cross-sectional shape indicates a robust magma supply but absence of an axial summit caldera, presumably due to recent flooding by lavas. There are only two "+" regions on the EPR between 9°N -13°N, these are the locations where volcanic eruptions were forecast (Macdonald and Fox, 1988). Most of the 9°45N-9°54N region has experienced post-1989 volcanism (Haymon *et al.*, 1991c), and a documented eruption ocurred in late March-early April 1991 near 9°51N (Haymon *et al.*, 1991b). ALVIN dives near 10°N in March 1992 document evidence for very recent volcanic activity here as well.

Figura 9.- Ampliación de la Fig. 2 de Macdonald y Fox (1988) en la que se ilustran los fundamentos de la predicción de la erupción de 1991. El perfil axial indica si el aporte de magma es abundante o escaso. La línea gruesa señala la localización del reflector sísmico de la cámara magmática axial (según Detrick *et al.*, 1987), la línea fina paralela al eje traza la caldera axial, y las cruces marcan las regiones en que el perfil transversal indica un aporte magmático abundante en ausencia de caldera somital axial. En la DOPE, entre 9°N y 13°N, sólo hay dos regiones con cruces, las cuáles se corresponden con los lugares en que se predijeron erupciones (Macdonald y Fox, 1988). En la mayor parte de la región entre 9°45N y 9°54N ha habido manifestaciones volcánicas después de 1989 (Haymon *et al.*, 1991c), produciéndose una erupción bien documentada cerca de 9°51N entre finales de Marzo y comienzos de Abril de 1991 (Haymon *et al.*, 1991b). Las inmersiones efectuadas por el ALVIN cerca de 10°N, en Marzo de 1992, también aportaron evidencias de actividad volcánica muy reciente en ese lugar.

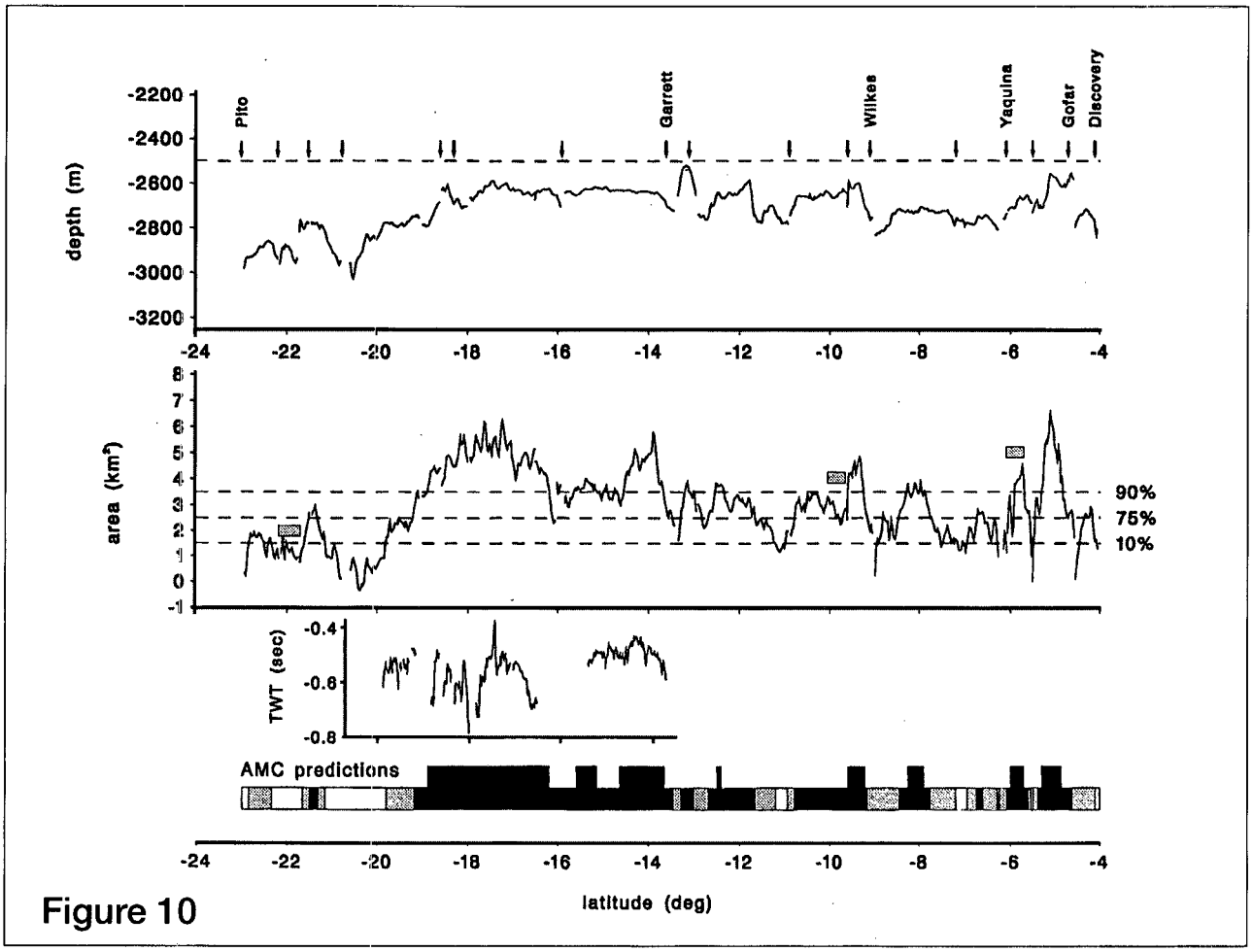

Figure 10

Figure 10.- Axial depth (top) and cross-sectional area (middle) profiles of the EPR 3°S-23°S from SeaMARCII and SeaBeam records; measurements taken every 1 km along strike. Bottom: Our predicions of magma chamber reflector locations beneath unsurveyed sections of the southern EPR (after Scheirer and Macdonald, in press; a full discussion of methods and results are given therein). Arrows indicate first and second order ridge axis discontinuities. Based on the documented relationship between occurrence of an axial magma chamber versus cross-sectional area 8°08N-13°N, portions of the ridge whose cross-sectional areas fall above the "90%" line (3.5 km^2) have 90% probability of having an axial magma chamber, same for the 75% and 10% lines. At the bottom of the figure, the tall, black stripes show where we are 90% confident that an AMC reflector exists; smaller black boxes show 75% confidence predictions for a reflector, and white areas indicate where we expect less than a 10% chance of a magma chamber event. Gray areas are intermediate levels, where we do not make a prediction about the presence or absence of an AMC reflector. We also expect that shallower and stronger magma chamber events would be observed beneath portions of the rise with the greatest cross-sectional area. The two-way travel time (TWTT) variation of the AMC reflector beneath the rise crest, displayed in the third panel, was digitized from Detrick *et al.*, (1993). Assuming a reasonable crustal velocity structure (Detrick *et al.*, 1993), the median depth of this AMC reflector beneath seafloor is about 1.3 km. A TWTT variation of 0.1s corresponds to a depth change of about 225 m. Our prediction agrees very well with the subsequent multi-channel seismic results.

Figura 10.- Perfiles de profundidad axial (arriba) y de áreas transversales (enmedio) entre 3°S y 23°S en la DOPE, construídos a partir de registros de SeaMARC II y SeaBeam. Las medidas se han efectuado a intervalos de 1 km siguiendo la dirección de la dorsal. En la parte inferior de la figura se muestran las predicciones acerca de la localización del reflector de la cámara magmática debajo de tramos no investigados de la DOPE meridional (de Scheirer y Macdonald, en prensa, artículo en el que se comentan detalladamente los métodos y resultados de tales predicciones). Las flechas señalan la posición de las discontinuidades axiales de primer y segundo orden. Basándose en la relación, probada entre 8°08N y 13°N, entre la ocurrencia de una cámara magmática axial y el área transversal, los tramos de dorsal cuyas áreas transversales se sitúan por encima de la "línea del 90%" (3,5 km^2) tienen un 90% de probabilidades de tener una cámara magmática axial. Y análogamente sucede para las líneas del 75% y del 10%. En la parte inferior de la figura, las bandas oscuras más altas ilustran los tramos en que se tiene un 90% de confianza acerca de la existencia de un reflector de CMA. Los tramos en negro más bajos indican un 75% de probabilidades de que exista dicho reflector, mientras que en los tramos en blanco las probabilidades de que se produzca un evento de cámara magmática son inferiores al 10%. Los tramos en gris representan niveles intermedios, en los que no se han efectuado predicciones acerca de la presencia o ausencia de un reflector de CMA. Es lógico esperar que los eventos de cámara magmática más someros e intensos sean observados en los tramos de dorsal con mayor área transversal. Las variaciones del reflector de CMA debajo de la cresta de la dorsal, dibujadas en tiempos dobles en el diagrama más pequeño de la figura, han sido digitalizadas a partir de Detrick *et al.* (1993). Aceptando una estructura cortical de velocidades razonable (Detrick *et al.*, 1993), resulta que la profundidad media de dicho reflector de CMA debajo del fondo marino es de unos 1,3 km. Una variación de 0,1 s en tiempos dobles equivale a un cambio de profundidad de unos 225 m. Las predicciones efectuadas concuerdan muy bien con los resultados de la sísmica de multicanal.

spreading EPR 13°S-20°S (Detrick *et al.*, 1991; Harding *et al.*, 1991). They showed that the magma chamber reflector is bright and narrow, and present along approximately 60% of the rise, very similar to the EPR 9°N-13°N observations. However, the reflector is shallower than 9°N-13°N (≈1 km) and at 17°20S, the reflector is less than 900 m beneath the seafloor (Detrick *et al.*, 1993)! When we presented the analysis of our first forecast for 9°45N-9°54N and the reasoning behind our next forecast for 17°20S-17°30S, Vincent Renard, who had conducted three reconnaissance dives with the French submersible CYANA in 1984 near 17°25S-17°27S (Renard *et al.*, 1985), related how they had seen large areas of fresh glassy lava, the same mysterious white bacterial mats blowing out of fissures in the lava carapace, and hydrothermal fluids venting straight out of cracks in the lava flow with no sulfide edifices developed yet; most of the same indicators of active eruption observed near 9°50N (Haymon *et al.*, 1991b). The sulfate/sulfide edifices grow in height at a rate of about 10 cm/day (Hekinian *et al.*, 1984), so this limits the age of the eruption to being very recent or ongoing. We think this is a second successful forecast of a deep seafloor volcanic eruption or perhaps a back-cast, an accepted practice in fly-fishing if not in volcanology. Subsequently, a preliminary analysis of March 1992 ALVIN dive observations near 10°N indicate that dike injection and minor volcanism may have occurred since 1991 in the 10°N-10°02N area (Macdonald, unpublished cruise report).

Recent seismic results also provided an opportunity to test our prediction of where axial magma chambers should be found between 3°S-23°S on the EPR (Fig. 10) (Macdonald and Fox, 1988). We refined this prediction by making a sequence of cross-sectional area calculations for the rise crest at 1 km intervals along strike using our digital bathymetric data base (Scheirer and Macdonald, 1991). At the Fall 1991 AGU, Detrick showed where the magma chamber had been imaged between 13°S-20°S (Detrick *et al.*, 1991). In Scheirer's talk, immediately following Detrick's, the predicted magma chamber locations, based on excessive or maximum cross-sectional area and shape, had a better than 80% agreement with seismic detection of a magma chamber reflector (we had only predicted occurrence, not depth or width of the magma chamber). Our earlier magma chamber prediction, based solely on shape of the axial high and presence of an axial summit caldera, was almost as succesful, and the predicted locations are published in Macdonald and Fox (1988) for comparison with the seismic results. Some of the axial relief we measure may be caused by variations in the thickness of the volcanic carapace (especially at ridges which spread at an intermediate rate), reflecting a longer term average of the magma supply than is measured seismically (Harding *et al.*, 1993). This is the most likely explanation for the 20% of the ridge where our prediction method fails.

While it is exciting to forecast submarine eruptions and the locations of magma chambers based on such a simple analysis of seafloor topography, the real scientific importance is not in the forecast itself but in the succesful test of two important hypotheses: (1) a distinctive morphology of the ridge axis is linked to the local magma supply, and (2) the fine-scale structure of the axial summit caldera is linked to the recent eruption history.

CONCLUSIONS

Precise mapping of the shape of the seafloor near mid-ocean ridges, in concert with other studies, has revealed a great deal about the genesis and tectonic processes responsible for the creation and evolution of oceanic crust. The mid-ocean ridge is segmented in a pattern which reflects magma supply. There is a hierarchy of segmentation such that short segments (≈10 km) tend to be short-lived (102-105 yrs), while long segments may last for millions of years. Presumably, the longer the segment, the deeper source (i.e. 1000 km long hot spot centers tap the lower mantle, intermediate wavelength expressions of segmentation several tens to hundreds of kilometers long tap sources in the upper mantle ≈50-60 km deep). The axial high at fast spreading centers is characterized by an axial summit caldera along its crest. The 300-400 m elevation of the high is produced by the buoyancy of hot rock and magma beneath the newly created edges of the spreading plates. The elevation is not a volcanic construction, so there is little vestige of it off-axis. At intermediate spreading rates, there is sufficicient cooling for a volcanic edifice to develop and sufficient thickening of the lithosphere on-axis for accumulation of strain and true normal faulting to occur. Splitting of axial volcanoes and axial grabens occur under these circumstances. Half-volcanoes, with their steep fault-bounded sides facing the spreading axis are preserved on the flanks of the ridge. Where axial rift valleys occur, at slow spreading centers and magma deficient intermediate-rate spreading centers, the neovolcanic zone lies within the inner floor of the rift valley. Numerous small conical volcanoes, which may coalesce into larger edifices, and elongated ridges created by fissure eruptions contribute to volcanic constructional terrain. On fast spreading ridges, the morphology and fine-scale structure of the ridge is sufficiently sensitive to magma supply to permit forecasts of magma chamber locations and even eruptions.

These are only a few examples taken largely from our own research of how useful precise measurements of seafloor topography can be. Many other examples could be cited; determining the history of and changes in plate motion; determining the relative importance of faulting, volcanism, sedimentation, and mass wasting in shaping the ocean floor; exploring the causes of linear seamount chains, and so on (e.g. Searle, 1992). Satellite measure-

ments have also provided low resolution glimpses of large uncharted areas of the seafloor (Marks *et al.*, 1991). While we have emphasized the importance of topographic measurements, marine geology/geophysics is very much an interdisciplinary area of research, and the charts and structural maps reviewed here provide a common base which draws together geochemists, seismologists, structural geologists and even biologists and chemists. Hopefully we will catch up with the successful mission to map the surface of Venus before the end of the millennium. The long term goal is the construction of a global-scale high resolution map of the seafloor that will define patterns of crustal evolution during the past 200 my and provoke fundamental insights into processes that shape the planet in space and time.

ACKNOWLEDGEMENTS

We thank ONR and NSF for the support of swath-mapping and ALVIN cruises which have made these observations possible, and appreciate reviews by R. Haymon. A shortened version of this paper appeared in GSA Today in the January and February, 1993 issues. Spanish abstract, and Table and figure captions have been translated by the editors.

REFERENCES

ATWATER, T., 1979: Constraints from the Famous area concerning the structure of the oceanic section. *In:* M. Talwani, C.G. Harrison and D.E. Hayes eds. *Deep Drilling Results in the Atlantic Ocean: Ocean Crust.* pp. 33-42, Washington, Maurice Ewing Series 2, AGU.

BALLARD, R.D. and VAN ANDEL, T.H., 1977: Morphology and tectonics of the inner rift valley at lat 36°50N on the Mid-Atlantic Ridge. *Geol. Soc. Am. Bull.*, 88: 507-530.

BICKNELL, J.D., SEMPERE, J.C., MACDONALD, K.C. and FOX, P.J., 1988: Tectonics of afast spreading center: A Deep-Tow and SeaBeam survey at EPR 19°30S. *Mar. Geophys. Res.*, 9: 25-46.

BLACKMAN, D.K. and FORSYTH, D.W., 1991: Isostatic compensation of tectonic features of the Mid-Atlantic Ridge: 25°S-27°30S. *J. Geophys. Res.*, 96: 11741-11758.

BRYAN, W.B. and MOORE, J.G., 1977: Compositional variations of young basalts on the Mid-Atlantic Ridge rift valley near 36°49N. *Geol. Soc. Am. Bull.*, 88: 556-570.

CARBOTTE, S.M and MACDONALD, K.C., 1990: Causes of variation in faulting-facing direction on the ocean floor. *Geology*, 18: 749-752.

CARBOTTE, S.M and MACDONALD, K.C., 1992: East Pacific Rise 8°N-10°30N: Evolution of ridge segments and discontinuities from SeaMARC II and three-dimensional magnetic studies. *J. Geophys. Res.*, 97: 6959-6982.

CHOUKROUNE, P., FRANCHETEAU, J. and HEKINIAN, R., 1984: Tectonics of the East Pacific Rise near 12°50N: A submersible study. *Earth Planet. Sci. Lett.*, 68: 115-127.

CHRISTESON, G.L., PURDY, G.M. and FRYER, G.J., 1992: Structure of young upper crust at the East Pacific Rise near 9°30N. *Geophys. Res. Lett.*, 19: 115-127.

COCHRAN, J.R., GOFF, J.A. MALINVERNO, A., FORNARI, D., KEELEY, J. and WANG, X., 1993: Morphology of a "superfast" mid-ocean ridge crest and flanks: The East Pacific Rise 7°S-9°S. *Mar. Geophys. Res.*, 15: 65-75.

CORMIER, M.H. and MACDONALD, K.C., 1991: Asymmetric spreading by rapid propagation of overlapping spreading centers. *EOS Trans. AGU*, 72: 506.

DAVIS, E.E., CURRIE, R.G., SAWYER, B.S. and KOSALOS, J.G., 1986: The use of swath bathymetric and acoustic image mapping tools in marine geoscience. *Mar. Technol. Soc. J.*, 20: 17-27.

DETRICK, R.S., BUHL, P., VERA, E., ORCUTT, J., MADSEN, J. and BROCHER, T., 1987: Multi-channel seismic imaging of a crustal magma chamber along the East Pacific Rise. *Nature*, 326: 35-41.

DETRICK, R.S., MUTTER, J.C., BUHL, P. and KIM, I.I., 1990: No evidence from multichannel reflection data for a crustal magma chamber in the MARK area on the Mid-Atlantic Ridge. *Nature*, 347: 61-63.

DETRICK, R.S., HARDING, A.J., ORCUTT, J., KENT, G., BUHL, P., MUTTER, J. and VERA, E., 1991: A two ship multi-channel seismic reflection and OBS experiment on the East Pacific Rise south of the Garrett fracture zone. *EOS Trans. AGU*, 72: 506.

DETRICK, R.S., HARDING, A.J., KENT, G.M., ORCUTT, J.A., MUTTER, J.C. and BUHL, P., 1993: Seismic structure of the southern East Pacific Rise. *Science*, 259: 499-503.

FOX, P.J. and GALLO, D.G., 1984: A tectonic model for ridge-transform-ridge plate boundaries: Implications for the structure of oceanic lithosphere. *Tectonophysics*, 104: 205-242.

FOX, P.J., GRINDLAY, N.R. and MACDONALD, K.C., 1991: The Mid-Atlantic Ridge (31°S-34°S): Temporal and spatial variations of accretionary processes. *Mar. Geophys. Res.*, 13: 1-20.

GRINDLAY, N.R., FOX, P.J. and MACDONALD, K.C., 1991: Second-order ridge axis discontinuities in the South Atlantic: Morphology, structure and evolution. *Mar. Geophys. Res.*, 13: 21-49.

HARDING, A.J., ORCUTT, J.A., KENT, G.M., DETRICK, R.S., MUTTER, J.C., BUHL, P. and VERA, E.E., 1991: Ocean bottom seismograph experiments at 14°15S, 15°55S, and 17°15S on the East Pacific Rise. *EOS Trans. AGU*, 72: 506.

HARDING, A.J., KENT, G.M. and ORCUTT, J.A., 1993: A multichannel seismic investigation of upper crustal structure at 9°N on the East Pacific Rise: Implications for crustal accretion. *J. Geophys. Res.*, 98: 13925-13944.

HAYMON, R.M., FORNARI, D.J., EDWARDS, M.H., CARBOTTE, S., WRIGHT, D. and MACDONALD, K.C., 1991a: Hydrothermal vent distribution along the East Pacific Rise crest (9°09N-9°54N) and its relationship to magmatic and tectonic processes on fast-spreading mid-ocean ridges. *Earth Planet. Sci. Lett.*, 104: 513-534.

HAYMON, R.M. and 17 others, 1991b: Eruption of the EPR crest at 9°45N-9°52N since late 1989 and its effects on hydrothermal venting: Results of the ADVENTURE Program, an ODP site survey with ALVIN. *EOS Trans. AGU,* 72: 480.

HAYMON, R.M. and 18 others, 1991c: Active eruption seen on East Pacific Rise. *EOS Trans. AGU,* 72: 505-507.

HAYMON, R.M. and 14 others, submitted: Volcanic eruption of the mid-ocean ridge along the East Pacific Rise crest at 9°45-9°52N: I. Direct submersible observations of seafloor phenomena associated with an eruption event in April, 1991. *Earth Planet. Sci. Lett.*

HEAD, J.W. and SAUNDERS, R.S., 1991: Geology of Venus: A perspective from early Magellan Mission results. *GSA Today,* 1: 49-60.

HEKINIAN, R., RENARD, V. and CHEMINEE, J.L., 1984: Hydrothermal deposits on the East Pacific Rise near 13°N: Geological setting and distribution of activew sulfide chimneys. *In:* P.A. Rona, K. Bostrom, L. Laubier and K. Smith eds. *Hydrothermal processes at spreading centers.* pp. 571-594, New York, Plenum Publ. Co.

KAPPEL, E.S. and RYAN, W.B.F., 1986: Volcanic episodicity and a non-steady state rift valley along norteast Pacific spreading centers: Evidence from SeaMARC I. *J. Geophys. Res.,* 91: 13925-13940.

KAPPUS, M.E., HARDING, J.A. and ORCUTT, J.A., 1992: Constraints on the support of axial topography along the East Pacific Rise based on the velocity structure of the upper crust. *EOS Trans. AGU,* 73: 274.

KONG, L.S.L., DETRICK, R.S., FOX, P.J., MAYER, L.A. and RYAN, W.B.F., 1988: The morphology and tectonics of the MARK area from SeaBeam and SeaMARC I observations. *Mar. Geophys. Res.,* 10: 59-90.

KUO, B.Y. and FORSYTH, D.W., 1988: Gravity anomalies of the Ridge-Transform system in the South Atlantic between 31°S and 34°30S: Upwelling centers and variations in crustal thickness. *Mar. Geophys. Res.,* 10: 205-232.

LANGMUIR, C.H., BENDER, J.F. and BATIZA, R., 1986: Petrological and tectonic segmentation of the East Pacific Rise, 5°30N-14°30N. *Nature,* 322: 422-429.

LIN, J., PURDY, G.M., SCHOUTEN, H., SEMPERE, J.C. and ZERVAS, C., 1990: Evidence from gravity data for focussed magmatic accretion along the Mid-Atlantic Ridge. *Nature,* 344: 627-632.

LIN, J. and PHIPPS MORGAN, J., 1992: The spreading rate dependence of three-dimensional mid-ocean ridge gravity structure. *Geophys. Res. Lett.,* 19: 13-16.

LONSDALE, P., 1977: Structural geomorphology of a fast-spreading rise crest: The East Pacific Rise near 3°25S. *Mar. Geophys. Res.,* 3: 251-293.

LONSDALE, P., 1985: Nontransform offsets of the Pacific-Cocos plate boundary and their traces on the rise flank. *Geol. Soc. Am. Bull.,* 96: 313-327.

LONSDALE, P., 1989: Segmentation of the Pacific-Nazca spreading center 1°N-20°S. *J. Geophys. Res.,* 94: 12197-12226.

LUYENDYK, B.P. and MACDONALD, K.C., 1985: A geological transect across the crest of the East Pacific Rise at 21°N latitude made from the deep submersible ALVIN. *Mar. Geophys. Res.,* 7: 467-488.

MACDONALD, K.C., 1982: Mid-Ocean Ridges: Fine scale tectonic, volcanic and hydrothermal processes within the plate boundary zone. *Ann. Rev. Earth Planet. Sci.,* 10: 155-190.

MACDONALD, K.C., 1986: The crest of the Mid-Atlantic Ridge: Models for crustal generation processes and tectonics. *In:* P.R. Vogt and B.E. Tucholke eds. *The Geology of North America. The Western North Atlantic Region.* Vol. M, pp. 51-68. Boulder, Colorado. Geol. Soc. Am.

MACDONALD, K.C., 1990: A slow but restless ridge. *Nature,* 348: 108-109.

MACDONALD, K.C., 1991: The East Pacific Ridge south of Garrett: Volcanic activity predicted for 14°-14°30S. *EOS Trans. AGU,* 72: 506.

MACDONALD, K.C. and FOX, P.J., 1988: The axial summit graben and cross-sectional shape of the East Pacific Rise as indicators of axial magma chambers and recent volcanic eruptions. *Earth Planet. Sci. Lett.,* 88: 119-131.

MACDONALD, K.C. and FOX, P.J., 1990: The mid-ocean ridge. *Scient. Am.,* 262: 72-79.

MACDONALD, K.C. and LUYENDYK, B.P., 1977: Deep-tow studies of the structure of the Mid-Atlantic Ridge crest near lat 37°N. *Geol. Soc. Am. Bull.,* 88: 621-636.

MACDONALD, K.C., MILLER, S.P., HUESTIS, S.P. and SPIESS, F.N., 1980: Three-dimensional modelling of a magnetic reversal boundary from inversion of deep-tow measurements. *J. Geophys. Res.,* 85: 3670-3680.

MACDONALD, K.C., MILLER, S.P., LUYENDYK, B.P., ATWATER, T.M. and SHURE, L., 1983: Investigation of a Vine-Matthews magnetic lineation from a submersible: The source and character of marine magnetic anomalies. *J. Geophys. Res.,* 88: 3403-3418.

MACDONALD, K.C., SEMPERE, J.C. and FOX, P.J., 1984: East Pacific Rise from Siqueiros to orozco fracture zones: Along-strike continuity of axial neovolcanic zone and structure and evolution of overlapping spreading centers. *J. Geophys. Res.,* 89: 6049-6069.

MACDONALD, K.C., SEMPERE, J.C., FOX, P.J. and TYCE, R., 1987: Tectonic evolution of rdige-axis discontinuities by the meeting, linking, or self-decapitation of neighboring ridge segments. *Geology,* 15: 993-997.

MACDONALD, K.C., FOX, P.J., PERRAM, L.J., EISEN, M.F., HAYMON, R.M., MILLER, S.P., CARBOTTE, S.M., CORMIER, M.H. and SHOR, A.N., 1988: A new view of the mid-ocean ridge from the behavior of ridge-axis discontinuities. *Nature,* 335: 217-225.

MACDONALD, K.C., HAYMON, R.M. and SHOR, A.N., 1989: A 220 km2 recently erupted lava field on the East Pacific Rise near 8°S. *Geology,* 17: 212-216.

MACDONALD, K.C., SCHEIRER, D.S. and CARBOTTE, S.M., 1991: Mid-ocean ridges: Discontinuities, segments and giant cracks. *Science,* 253: 986-994.

MACDONALD, K.C., FOX, P.J., MILLER, S.P., CARBOTTE, S.M., EDWARDS, M., EISEN, M., FORNARI, D.J., PERRAM, L.J., POCKALNY, R., SCHEIRER, D., TIGHE, S., WEILAND, C. and WILSON, D., 1992: The East Pacific Rise and its flanks 8°N-18°N: History of segmentation, propagation and spreading direction based on SeaMARC II and SeaBeam studies. *Mar. Geophys. Res.*, 14: 299-344.

MARKS, K.M., MCADOO, D.C. and SANDWELL, D.T., 1991: Geosat GM data reveal new details of ocean floor. *EOS Trans. AGU*, 72: 145-149.

NORMARK, W.R., 1976: Delineation of the main extrusion zone of the East Pacific Rise at lat 21°N. *Geology*, 4: 681-685.

PERRAM, L.J. and MACDONALD, K.C., 1990: A one-million-year history of the 11°45N East Pacific Rise discontinuity. *J. Geophys. Res.*, 95: 21363-21381.

POCKALNY, R.A., DETRICK, R.S. and FOX, P.J., 1988: Morphology and tectonics of the Kane transform from SeaBeam bathymetric data. *J. Geophys. Res.*, 93: 3179-3193.

PURDY, G.M., KONG, L.S.L., CHRISTESON, G.L. and SOLOMON, S.C., 1992: Relationship between spreading rate and the seismic structure of mid-ocean ridges. *Nature*, 355: 815-817.

RENARD, V., HEKINIAN, R., FRANCHETEAU, J., BALLARD, R.D. and BACKER, H., 1985: Submersible observations at the axis of the ultra-fast spreading East Pacific Rise (17°30S to 21°30S). *Earth Planet. Sci. Lett.*, 75: 339-353.

RENARD, V., VOISSET, M. and NEEDHAM, H.D., 1991: The research vessel L'Atalante's mapping system: The EM12 dual echosounder. Evaluation of its performance for mid-oceanic ridge bathymetric investigations. *EOS Trans. AGU*, 72: 470.

ROHR, K.M.M., PURDY, G.M. and MIKEREIT, B., 1992: Upper oceanic crust: laterally homogeneous or heterogeneous? *EOS Trans. AGU*, 73: 274.

RUBIN, K.H. and MACDOUGALL, J.D., 1991: Fine chronology of recent mid-ocean ridge eruptions on the southern JDF and 9°N EPR from 226Ra-230Th-238U and 210Po-210Pb disequilibrium. *EOS Trans. AGU*, 72: 231.

SCHEIRER, D.S. and MACDONALD, K.C., 1991: Variation of the axial cross-sectional area along the northern and southern East Pacific Rise. *EOS Trans. AGU*, 72: 506.

SCHEIRER, D.S. and MACDONALD, K.C., in press: The variation in cross-sectional area of the axial ridge along the East pacific Rise: Evidence for the magmatic budget of a fast-spreading center. *J. Geophys. Res.*

SCHOUTEN, H., KLITGORD, K.D. and WHITEHEAD, J.A., 1985: Segmentation of mid-ocean ridges. *Nature*, 317: 225-229.

SCLATER, J.G., ANDERSON, R.N. and BELL, M.L., 1971: The elevation of ridges and the evolution of the central Pacific. *J. Geophys. Res.*, 76: 7888-7915.

SEARLE, R.C., 1984: GLORIA survey of the East Pacific Rise near 3°30S: Tectonic and volcanic characteristics of a fast spreading mid-ocean rise. *Tectonophysics*, 101: 319-344.

SEARLE, R.C., 1992: The volcano-tectonic setting of oceanic lithosphere generation. *In:* L.M. Parson, B.J. Murton and P. Browning eds. *Ophiolites and their modern oceanic analogues*. pp. 65-79. Geol. Soc. London Sp. Publ., No 60.

SEARLE, R.C. and LAUGHTON, A.S., 1977: Sonar studies of the Mid-Atlantic Ridge and Kurchatov fracture zone. *J. Geophys. Res.*, 82: 5313-5328.

SEMPERE, J.C., PURDY, G.M. and SCHOUTEN, H., 1990: Segmentation of the Mid-Atlantic Ridge between 24°N and 30°40N. *Nature*, 344: 427-431.

SEMPERE, J.C., PALMER, J., CHRISTIE, D.M., PHIPPS MORGAN, J. and SHOR, A.N., 1991: Australian-Antarctic discordance. *Geology*, 19: 429-432.

SINTON, J.M. and DETRICK, R.S., 1992: Mid-ocean ridge magma chambers. *J. Geophys. Res.*, 97: 197-216.

SMITH, D.K. and CANN, J.R., 1990: Hundreds of small volcanoes on the median valley floor of the Mid-Atlantic Ridge at 24°-30°N. *Nature*, 348: 1523-1525.

SMITH, D.K. and CANN, J.R., 1992: The role of seamount volcanism in crustal construction at the Mid-Atlantic Ridge (24°-30°N). *J. Geophys. Res.*, 97: 1645-1658.

SOLOMON, S.C. and TOOMEY, D.R., 1992: The structure of mid-ocean ridges. *Ann. Rev. Earth Planet. Sci.*, 20: 329-364.

SPIESS, F.N. and TYCE, R.C., 1973: Marine physical laboratory deep tow instrumentation system. *SIO* . Ref. 73-4, 73 p.

TIGHE, S.A and FOX, P.J., 1991: Formation of abyssal hills at fast spreading centers by axial volcanic subsegments. *EOS Trans. AGU*, 72: 465-466.

TOOMEY, D.R., PURDY, G.M., SOLOMON, S.C. and WILCOCK, W.S.D., 1990: The three-dimensional seismic velocity structure of the East Pacific Rise near latitude 9°30N. *Nature*, 347: 639-645.

TYCE, R.C., 1987: Deep seafloor mapping systems - A review. *Mar. Technol. Soc. J.*, 20: 4-16.

VERA, E.E., MUTTER, J.C., BUHL, P., ORCUTT, J.A., HARDING, A.J., KAPPUS, M.E., DETRICK, R.S. and BROCHER, T.M., 1990: The structure of 0 to 0.2 my old oceanic crust at 9°N on the East Pacific Rise from expanded spread profiles. *J. Geophys. Res.*, 95: 15529-15556.

WILSON, D.S., 1990: Kinematics of overlapping rift propagation with cyclic rift failure. *Earth Planet. Sci. Lett.*, 96: 384-392.